

# TTCM-Aided Rate-Adaptive Distributed Source Coding for Rayleigh Fading Channels

Abdulah Jeza Aljohani, Soon Xin Ng, *Senior Member, IEEE*, and Lajos Hanzo, *Fellow, IEEE*

**Abstract**—Adaptive turbo-trellis-coded modulation (TTCM)-aided asymmetric distributed source coding (DSC) is proposed, where two correlated sources are transmitted to a destination node. The first source sequence is TTCM encoded and is further compressed before it is transmitted through a Rayleigh fading channel, whereas the second source signal is assumed to be perfectly decoded and, hence, to be flawlessly shown at the destination for exploitation as side information for improving the decoding performance of the first source. The proposed scheme is capable of reliable communications within 0.80 dB of the Slepian–Wolf/Shannon (SW/S) theoretical limit at a bit error rate (BER) of  $10^{-5}$ . Furthermore, its encoder is capable of accommodating time-variant short-term correlation between the two sources.

**Index Terms**—Distributed source coding (DSC), joint source-channel coding, Slepian–Wolf (SW) coding, Turbo-trellis-coded modulation (TTCM).

## I. INTRODUCTION

DISTRIBUTED source coding (DSC) [1] refers to the problem of compressing several physically separated, but correlated sources, where the receiver can perform joint decoding of both encoded signals. The schematic of asymmetric DSC [2] is shown in Fig. 1, where source sequence  $\{b_1\}$  is compressed before its transmission, whereas the correlated source signal  $\{b_2\}$  is assumed to be available at the decoder but not at the source  $\{b_1\}$ . More explicitly, the encoder has to compress  $\{b_1\}$  without knowing  $\{b_2\}$ , yet the decoder is capable of exploiting the knowledge of  $\{b_2\}$  for recovering  $\{b_1\}$ .

More explicitly, the Slepian–Wolf (SW) [3] coding theorem specifies the achievable rate regions of the compressed correlated sources  $\{b_1\}$  and  $\{b_2\}$  for transmission to a joint decoder as  $R_1 \geq H(b_1|b_2)$ ,  $R_2 \geq H(b_2|b_1)$ , and  $R_1 + R_2 \geq H(b_1, b_2)$ , where  $H(b_1|b_2)$  and  $H(b_1, b_2)$  denote the conditional entropy and joint entropy, respectively. Remarkably, this bound is identical, regardless whether joint encoding or joint decoding is used, i.e., regardless of where the joint processing takes

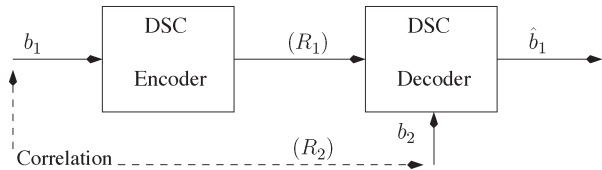


Fig. 1. Schematic of the asymmetric DSC.

place. This is quite convenient for exploiting the correlation of sources, which are distant from each other with the aid of joint processing at the receiver. This would facilitate for example the efficient joint decoding of correlated camera-phone-video sequences at the base station, namely, sequences, which portray the same scene from different angles.

This promising theoretical result has led to an increasing interest in a variety of applications, such as sensor networks [1], robust wireless video transmission [4], and compression of secure biometric data [5], where exchanging information between source nodes is not possible or not practical. Applying DSC techniques in wireless sensor networks, for example, has led to a new processing paradigm, where the potential computational complexity has been moved from the battery-limited sources to the central decoder connected to the mains supply.

As a consequence, the critical power constraint, which directly predetermines the life span of the wireless node, is fulfilled [1]. The first practical DSC technique was proposed in [6], where both sources  $\{b_1\}$  and  $\{b_2\}$  are assumed to be emitting equiprobable codewords, but they exhibit a difference because  $\{b_2\}$  is known only to the joint decoder but not to the encoder of  $\{b_1\}$ . Naturally, this assumption does not preclude that the codewords of  $\{b_2\}$  actually received from a remote source, but they must be first perfectly recovered in isolation before they may be used by the joint decoder for recovering  $\{b_1\}$ . Then, the codewords of both sources are grouped in cosets, where the members of each coset are separated by the maximum possible Hamming distance. Given  $\{b_2\}$  at the receiver, it is sufficient to transmit the index of the specific coset hosting the codewords of  $\{b_1\}$ . The decoder then estimates the transmitted codeword by choosing the one that is closest to the side information constituted by  $\{b_2\}$  of a given coset in terms of the Hamming distance.

The idea of using channel coding techniques<sup>1</sup> has enabled practical solutions to be developed. Practical Slepian–Wolf

Manuscript received July 8, 2013; revised September 30, 2013; accepted October 1, 2013. This work was supported in part by the Ministry of Higher Education of Saudi Arabia, by the European Union's Seventh Framework Programme through the CONCERTO Project under Grant 288502, by the Research Councils U.K. through the India–U.K. Advanced Technology Centre, by the European Research Council under an Advanced Fellow Grant, and by the Royal Society under the Wolfson Research Merit Award. The review of this paper was coordinated by Dr. E. K. S. Au.

The authors are with the Communications, Signal Processing, and Control Research Group, School of Electronics and Computer Science, University of Southampton, Southampton SO17 1BJ, U.K. (e-mail: ajra1c09@ecs.soton.ac.uk; sxn@ecs.soton.ac.uk; lh@ecs.soton.ac.uk).

Color versions of one or more of the figures in this paper are available online at <http://ieeexplore.ieee.org>.

Digital Object Identifier 10.1109/TVT.2013.2285020

<sup>1</sup>Since the correlation between the sources may be interpreted as the ameliorating effect of a “virtual” channel, a good channel code having, for example, a maximum minimum Hamming distance will be a good SW code [7].

76 schemes using turbo codes (TCs) were proposed for example  
 77 in [2], [8], and [9], whereas low-density parity-check (LDPC)  
 78 codes were considered in [10]–[12]. However, finding the best  
 79 code for approaching the Slepian–Wolf/Shannon (SW/S) limit  
 80 was not considered in [2], [8], and [9]. Later, a so-called “super”  
 81 TC was proposed in [13], aiming for approaching the SW/S  
 82 limit, when communicating over additive white Gaussian noise  
 83 (AWGN) channels. However, the scheme proposed in [13] for  
 84 an AWGN channel suffers from an error floor when communi-  
 85 cating over Rayleigh fading channels that makes the system less  
 86 suitable for wireless applications. A modified LDPC code was  
 87 proposed in [14] for mitigating the error floor, but nonetheless,  
 88 a high error floor persists when the correlation between the  
 89 sources is low. A joint turbo equalizer and decoder scheme  
 90 was proposed for asymmetric DSC in [15], whereas an iterative  
 91 joint turbo equalizer and decoder scheme was conceived for  
 92 transmission over a multipath Rayleigh fading multiple-access  
 93 channel in [16]. Both schemes have achieved a near-SW/S  
 94 performance, albeit at high joint decoding complexity. More  
 95 specifically, 35 iterations were invoked between the decoder  
 96 components in [15], whereas as many as 350 iterations were  
 97 required in [16] for attaining a near-SW/S performance. By  
 98 contrast, we only invoke eight turbo iterations in our TTCM  
 99 decoder, where both constituent decoders have comparable  
 100 complexity [17].

101 Furthermore, in practice, the short-term correlation among  
 102 the sources might be time variant; hence, adaptive-rate schemes  
 103 have to be considered, where the code rate is controlled via  
 104 a feedback channel. More specifically, if the bit error rate  
 105 (BER) evaluated after decoding exceeds a given threshold,  
 106 more syndromes (or parity bits if parity puncturing is used)  
 107 will be requested from the transmitter. A pair of innovative  
 108 adaptive-rate LDPC schemes was proposed in [18], whereas  
 109 adaptive-rate TCs were designed in [19]. In [18], the encoder  
 110 stored the syndromes and incrementally transmitted them to  
 111 the receiver, when the decoder failed to find the legitimate  
 112 codeword. Both papers considered an asymmetric DSC struc-  
 113 ture based on the puncturing of the syndrome generated by the  
 114 channel encoders, while stipulating the idealized simplifying  
 115 assumption of modeling the channel as the parallel combination  
 116 of a perfect channel and a binary symmetric channel (BSC).  
 117 More advanced adaptive-rate schemes considered the employ-  
 118 ment of a polar code [20] or efficient particle-based belief-  
 119 propagation-aided decoding [21] and density-evolution-based  
 120 decoding techniques [18].

121 Against this background, we propose a novel bandwidth-  
 122 efficient turbo-trellis-coded modulation (TTCM) scheme,  
 123 which combines the functions of coding and modulation for  
 124 conceiving a new DSCs system. TTCM [22] has a structure  
 125 similar to that of the family of binary TCs, where two identical  
 126 parallel-concatenated TCM schemes rather than conventional  
 127 codes are employed as component codes. The classic TTCM  
 128 design was outlined in [22], which is based on the search for  
 129 the best TCM component codes using the so-called “punctured”  
 130 minimal distance criterion, to approach the capacity of the  
 131 AWGN channel. The TTCM code advocated was designed to  
 132 improve the attainable throughput by considering the design of  
 133 error-correcting code and modulation where the parity bits are

absorbed in without any bandwidth expansion by increasing  
 the number of bits per modulated symbol. By contrast, all  
 separated channel codes, such as turbo or LDPC codes, impose  
 a bandwidth expansion, which is proportional to the code rate.  
 Furthermore, a novel adaptive-rate mechanism is conceived for  
 increasing the system’s effective throughput, while ensuring an  
 infinitesimally low BER. Hence, our new contributions are as  
 follows.

- We propose a uniquely amalgamated DSC and TTCM (DSTTCM) scheme for SW coding, which is capable of attaining a near-SW/S performance for a wide range of source correlation values. Our new scheme exhibits no error floor,<sup>2</sup> despite its low complexity. Furthermore, a carefully constructed modified symbol-based maximum *a posteriori* (MAP) algorithm is conceived for exploiting the side information available at the decoder. Additionally, we eliminate the aforementioned idealized simplifying assumptions exploited in the prior literature [18], [19], [23], and consider more realistic uncorrelated Rayleigh fading channels and BSCs.
- Furthermore, adaptive DSTTCM (A-DSTTCM) is proposed for accommodating the near-instantaneously time-varying nature of the wireless channel and the short-term correlation fluctuations among the sources. More explicitly, the system adapts its parameters according to both the channel quality and the correlation  $\rho$  of the sources,<sup>3</sup> while maintaining a given target BER.

The remainder of this paper is organized as follows. The proposed system model is described in Section II. The proposed scheme is designed in Section III. Section IV discusses our results. Finally, our conclusions are offered in Section V.

## II. SYSTEM MODEL

The asymmetric DSC scenario in Fig. 1 was considered here, where sequence  $\{b_2\}$  is transmitted at the rate of  $R_2 = H(b_2)$ , which is typically referred to as “side information” in most contributions [2], [8]; again, however, it can be also interpreted as another desired source signal, which was perfectly recovered. Sequence  $\{b_2\}$  can be also transmitted through an independent Rayleigh-fading channel, in which case, a similar encoder structure to that of the first source  $\{b_1\}$  has to be implemented/ The problem in this scenario may be considered a symmetric DSC one. Symmetric DSC compression was discussed, for example, in [13], [14], and [16], but due to space limitations, it is beyond the scope of this paper.

Furthermore, crossover probability  $p_e$  used for modeling correlation parameter  $\rho$  may be assumed to be the overall probability of error, which is denoted as  $p_{e_1}$  and  $p_{e_2}$ . More explicitly, the error between the two sources is denoted by  $p_{e_1}$  and  $p_{e_2}$  which characterizes the transmission error between the second source and the destination. Thus, in this scenario, the overall error obeys  $p_e \leq p_{e_1} + p_{e_2}$ . The correlated sequence  $\{b_1\}$  is then compressed for approaching the Slepian–Wolf bound to a

<sup>2</sup>As documented in Fig. 4, no error floor is observed at above BER level of  $10^{-6}$ ; hence, our scheme is evidently suitable for wireless applications.

<sup>3</sup> $\rho$  is expressed using a crossover probability  $p_e$  as  $\rho = 1 - 2p_e$ .

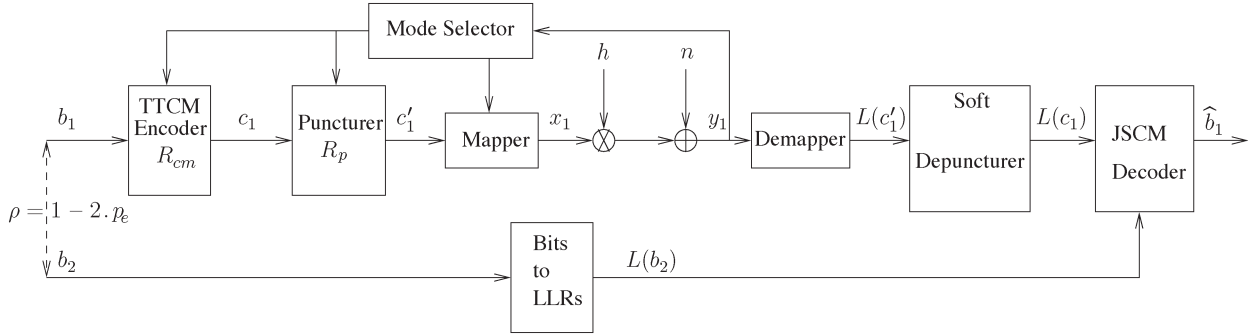


Fig. 2. Block diagram of the A-DSTTCM system communicating over Rayleigh fading channels. Sources  $\{b_1\}$  and  $\{b_2\}$  are assumed to be correlated, i.e., we have  $H(b_1 | b_2) \neq H(b_1)$ , and  $L(\cdot)$  denotes the LLRs.

186 rate of  $R_1 = H(b_1|b_2)$  to achieve the overall rate of  $H(b_1, b_2)$ .  
 187 Typically, the BSC is used for modeling the correlation between  
 188 the two source sequences  $\{b_1\} = \{b_1^1, b_1^2, \dots, b_1^i, \dots, b_1^N\}$  and  
 189  $\{b_2\} = \{b_2^1, b_2^2, \dots, b_2^i, \dots, b_2^N\}$ , where  $N$  is the length of each  
 190 source block.

191 For example, when  $\{b_1\}$  and  $\{b_2\}$  have a correlation of  
 192  $\rho = 0.9$  given the perfect knowledge of  $\{b_2\}$ ,  $\{b_1\}$  may be in-  
 193 terpreted as the output signal of BSC, which was contaminated  
 194 by the bit-flipping error events occurring with a probability  
 195 of  $p_e$ . Source sequence  $\{b_1\}$  is generated by an equiprobable  
 196 binary symmetric independent identically distributed (i.i.d.)  
 197 source, whereas  $\{b_2\}$  can be defined as  $b_1^i = b_2^i \oplus e_i$ , where  $\oplus$   
 198 is the modulo-2 addition operation, and  $e_i$  is an independent  
 199 binary random variable assuming the logical value of 1 with  
 200 a crossover probability of  $p_e$  and of 0 with a probability of  
 201  $(1 - p_e)$ . Both the random variables of  $b_1^i$  and  $b_2^i$  in the pair  
 202 of bit streams  $\{b_1\}$  and  $\{b_2\}$  may be assumed to be i.i.d. for  
 203 the bit index  $i$ ; hence, both sources emit equiprobable [16] bits.  
 204 Consequently, the entropy of each source is unity, which yields  
 205 conditional entropy of

$$\begin{aligned}
 H(p_e) &= H(b_1|b_2) \\
 &= \lim_{i \rightarrow \infty} \frac{1}{i} H((b_1^1, \dots, b_1^i, \dots, b_1^N) | (b_1^2, \dots, b_1^i, \dots, b_1^N))
 \end{aligned}
 \tag{1}$$

206 where  $H(p_e) = p_e \log_2(1/p_e) + (1 - p_e) \log_2(1/(1 - p_e))$  is  
 207 the entropy of the binary random variable, and  $e_i$  is used for  
 208 parametrizing the side information/ Therefore, the achievable  
 209 SW rate region is given by the following three inequalities [16]:

$$\begin{aligned}
 R_1 &\geq H(p_e) \\
 R_2 &\geq H(p_e) \\
 R_1 + R_2 &\geq 1 + H(p_e).
 \end{aligned}
 \tag{2}$$

210 Let us now embark on the design of a joint source-channel  
 211 (JSC) decoding scheme for minimizing the signal-to-noise  
 212 power ratio (SNR) required for approaching the SW/S bound,  
 213 while maintaining reliable communications. More explicitly,  
 214 let us define  $\text{SNR} = R_1 \cdot E_b/N_0$ , where  $E_b/N_0$  denotes the  
 215 energy per bit to noise power spectral density.

### A. Encoder

216

The block diagram of the proposed A-DSTTCM scheme con- 217  
 sidered for transmitting correlated sources is shown in Fig. 2, 218  
 where  $L(\cdot)$  denotes the log-likelihood ratios (LLRs) of the bits. 219  
 As shown in Fig. 2, the input sequence  $\{b_1\}$  is fed into a 220  
 TTCM encoder, which has a coding rate of  $R_{cm} = m/m + 1$  221  
 and invokes a  $2^{m+1}$ -level modulation scheme. The TTCM- 222  
 encoded bits are then punctured at a rate of  $R_p$ . The resultant bit 223  
 sequence  $\{c'_1\}$  is then mapped to the corresponding modulated 224  
 symbols  $\{x_1\}$  before their transmission over an uncorrelated 225  
 Rayleigh fading channel. The second bit sequence  $\{b_2\}$  will 226  
 be converted to the LLRs  $L(b_2) = L_e$ , which is then will be 227  
 exploited as side information. This conversion is necessary 228  
 because the joint decoder is a soft-decision-based one. These 229  
 LLRs are characterized by the aforementioned crossover prob- 230  
 ability  $p_e$  and can be estimated as 231

$$\begin{aligned}
 L(b_2|b_1) &= \ln \left[ \frac{\Pr(b_2 = +1|b_1)}{\Pr(b_2 = -1|b_1)} \right] \\
 &= \ln \left[ \frac{(1 - p_e) \Pr(b_1 = +1) + p_e \Pr(b_1 = -1)}{(1 - p_e) \Pr(b_1 = -1) + p_e \Pr(b_1 = +1)} \right].
 \end{aligned}
 \tag{3}$$

We assume that these LLRs are available at the destination 232  
 and to be exploited by the joint decoder, whereas  $p_e$  can be 233  
 estimated at the decoder using (11). 234

As an example, we use a rate  $R_{cm} = 1/2$  TTCM encoder 235  
 relying on a puncturer of rate  $R_p = 2/1$ , which punctures 236  
 one bit out of two encoded bits. We assume that all the 237  
 systematic bits are punctured, whereas all the parity bits are 238  
 transmitted to the decoder. Hence, the overall code rate is 239  
 $R_1 = R_{cm} \cdot R_p = 1$ . However, the parity bit sequence may be 240  
 also further punctured to achieve an increased compression 241  
 ratio. The resultant bits are then mapped to binary phase-shift 242  
 keying (BPSK) symbols, i.e., the modulation mode has been 243  
 changed from quadrature phase-shift keying (QPSK) to BPSK 244  
 (QPSK/BPSK). Thus, the corresponding effective throughput 245  
 is given by  $\eta = R_1 \cdot \log_2(2) = 1$  bits per symbol (BPS). Then, 246  
 the modulated symbol sequence  $\{x_1\}$  is transmitted over an 247  
 uncorrelated Rayleigh fading channel, and the received symbol 248  
 $y_1$  is given by 249

$$y_1 = hx_1 + n \tag{4}$$

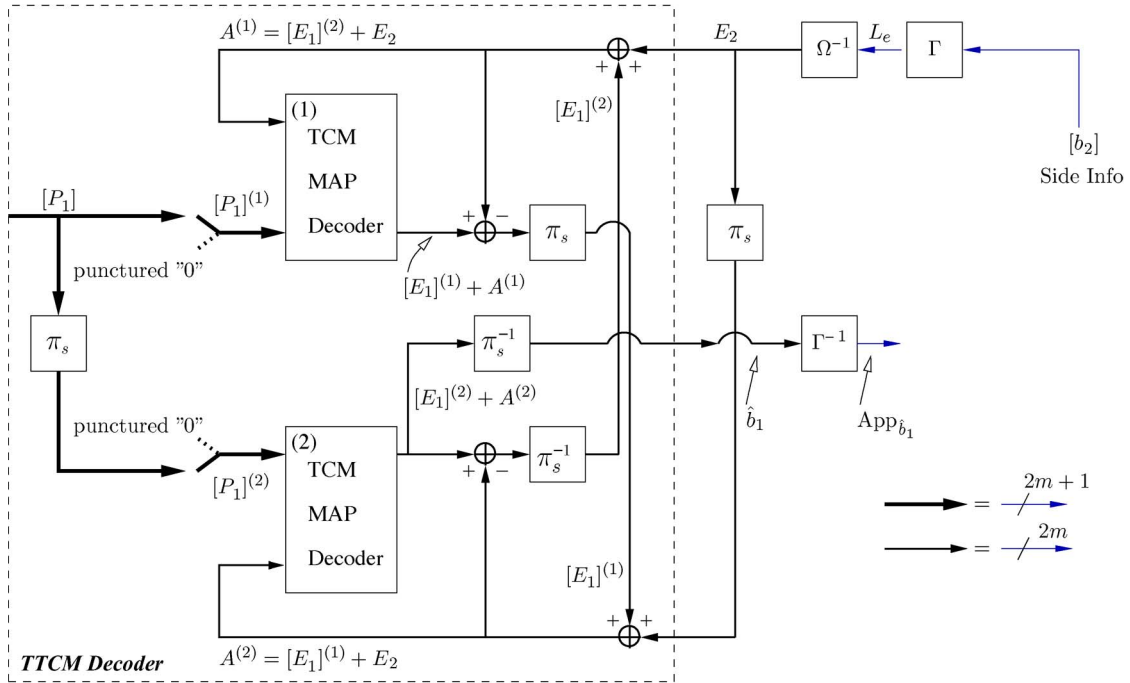


Fig. 3. Block diagram of the JSC-aided TTCM decoder conceived for our DSC system. Notations  $\pi_s$  and  $\pi_s^{-1}$  represent the symbol interleaver and deinterleaver, respectively, whereas  $\Gamma$  and  $\Gamma^{-1}$  denote the relevant symbol-to-LLR and LLR-to-symbol probability conversion.

250 where  $h$  is the fading coefficient of the channel, and  $n$  is the  
251 AWGN having a variance of  $N_0/2$  per dimension. The short-  
252 term average received SNR is given by

$$\text{SNR}_r = \frac{E\{|h|^2\}E\{|x_1|^2\}}{N_0} \quad (5)$$

253 where  $x_1$  represents the modulated symbols of source  $\{b_1\}$   
254 after puncturing. Furthermore, we have  $E\{|x_1|^2\} = 1$ , and  
255 the SNR of  $\gamma_r = 10 \log_{10}(|h|^2/N_0)$  [dB] is estimated for each  
256 received block. Note that  $\{b_2\}$  is related to  $\{b_1\}$  according  
257 to  $b_1^i = b_2^i \oplus e_i$ , as detailed in Section II. Diverse effective  
258 throughputs may be derived by changing  $R_{cm}$  and  $R_p$ ; hence,  
259 the proposed scheme exhibits substantial flexibility. In our  
260 A-DSTTCM scheme, the following modes are chosen at the  
261 encoder to ensure that  $\text{BER} < 10^{-5}$ :

- 262 • No transmission;
- 263 • DSTTCM-QPSK/BPSK;
- 264 • DSTTCM-8PSK/QPSK;
- 265 • DSTTCM-16-quadrature amplitude modulation (QAM)/  
266 8PSK;
- 267 • DSTTCM-32QAM/16QAM.

268 Thus, the effective throughput of our adaptive system as-  
269 sumes the values of  $\eta = \{0, 1, 2, 3, 4\}$  BPS.

### 270 B. Joint Source–Channel Decoder

271 Our JSC-decoding-aided DSTTCM scheme is shown in  
272 Fig. 3. Both TCM decoders invoke the symbol-based MAP  
273 algorithm [17] operating in the logarithmic domain. The TCM  
274 decoders are labeled with the round-bracketed indexes, whereas  
275 the notation  $P$ ,  $A$ , and  $E$  denote the logarithmic probabilities  
276 of the *a posteriori*, *a priori*, and *extrinsic* information, respec-  
277 tively, where  $L_e = L(b_2|b_1)$ . The  $2^{(m+1)}$ -ary  $P$  probabilities

associated with a specific  $(m+1)$ -bit TTCM-coded symbol 278  
 $\{c_1'\}$  are fed into the TTCM MAP decoder. A pair of signal 279  
components is generated by the constituent TCM decoders [17]; 280  
specifically, the *extrinsic* probability  $E$  is generated by each 281  
of the TCM decoders, whereas the *a priori* probability  $A$  is 282  
gleaned by each TCM decoder from the other one. Furthermore, 283  
as shown in Fig. 3, the additional *extrinsic* probability  $E_2$  284  
extracted from the side information  $\{b_2\}$  is also added to 285  
the *a priori* probability  $A$ , yielding  $A^{(1,2)} = [E_1]^{(2,1)} + E_2$ . 286  
Each of the constituent TCM blocks in Fig. 3 calculates the 287  
*a posteriori* probabilities using the forward and backward re- 288  
cursion methods.<sup>4</sup> 289

Upon recalling (4), we are now in the position to formulate 290  
the channel's transition metric as 291

$$\eta_i(\dot{s}, s) = \ln \left\{ \frac{1}{\pi N_0} e^{-|y_1 - h x_1|^2 / N_0} \right\}. \quad (6)$$

Then, both the backward and forward recursion methods of 292  
[17] are invoked for calculating  $\beta_{i-1}(\dot{s})$  and  $\alpha_i(s)$  as follows: 293

$$\alpha_i(s) = \max_{\dot{s}}^* (\alpha_{i-1}(\dot{s}) + \eta_i(\dot{s}, s) + A^{(1,2)}) \quad (7)$$

$$\beta_{i-1}(\dot{s}) = \max_s^* (\beta_i(s) + \eta_i(\dot{s}, s) + A^{(1,2)}) \quad (8)$$

where  $\max^*$  represents the Jacobian logarithm [17] evaluating 294  
all variables in the logarithmic domain, with  $(\dot{s}, s)$  denoting the 295  
transitions emerging from the previous state  $\dot{s}$  to the present 296  
state  $s$ . 297

<sup>4</sup>Detailed descriptions can be found in [17, Sec. 14.3]. Note that we illustrate the MAP process in the logarithmic domain to render it compatible with Fig. 3.

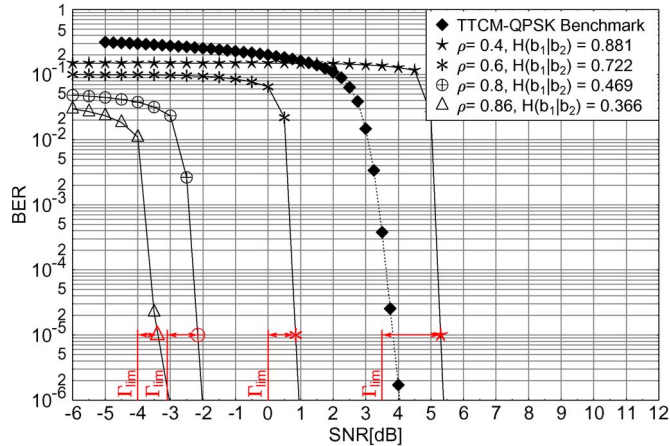


Fig. 4. BER versus SNR performance of the proposed DSTTCM-QPSK/BPSK scheme for correlation parameters of  $\rho = \{0.4, 0.6, 0.8, 0.86\}$  when transmitting over uncorrelated Rayleigh fading channels. The number of decoding iterations is  $I = 8$ .

### 298 III. RATE REGION DESIGN AND ANALYSIS

299 The achieved rate region experienced in a noisy channel for  
300 both sources is given by [13], [16]:

$$\begin{aligned} H(b_1, b_2) &\leq \frac{C_1}{R_1} + \frac{C_2}{R_2} \\ &\leq \frac{1}{R_1} E \{ \log_2(1 + \gamma_1) \} + \frac{1}{R_2} E \{ \log_2(1 + \gamma_2) \} \end{aligned} \quad (9)$$

301 where  $C_1 = E \{ \log_2(1 + \gamma_1) \}$  and  $C_2 = E \{ \log_2(1 + \gamma_2) \}$  de-  
302 note the ergodic channel capacities between each of the sources  
303 and the destination, whereas  $\gamma_1$  and  $\gamma_2$  denote the correspond-  
304 ing received SNRs. In our asymmetric system, we assume  
305 that  $\{b_2\}$  is transmitted at  $R_2 = H(b_2) = 1$ , whereas we aim  
306 for compressing  $\{b_1\}$  to its minimum rate, namely, to  $R_1 =$   
307  $H(b_1|b_2)$ . Then, based on (9), the effective throughput of our  
308 scheme for the  $\{b_1\}$  link can be expressed as  $\eta_{SW} = R_1 \cdot$   
309  $H(b_1|b_2)$ , whereas the SW/S bound is calculated as [15]

$$R_1 \cdot H(b_1|b_2) \leq C_1 \quad (10)$$

310 where  $C_1$  represents the ergodic capacity of the uncorrelated  
311 Rayleigh fading channel.

312 First we characterize the BER performance of our DSTTCM-  
313 QPSK/BPSK scheme employing a range of correlations  $\rho =$   
314  $\{0.4, 0.6, 0.8, 0.86\}$ . We opted for using 1/2-rate TCM for  
315 encoding a block of  $N_S = 12\,000$  symbols, resulting in  $N_b =$   
316  $24\,000$  bits before we remove all of the systematic bits from  
317 the TCM-coded sequence with the aid of puncturing. The  
318 BER versus SNR performance of the proposed system is shown  
319 in Fig. 4. Note that the SNR can be calculated in decibels  
320 as  $\text{SNR}(\text{dB}) = E_b/N_0(\text{dB}) + 10 \log(R_1)$ . The minimum SNR  
321  $\Gamma_{\text{lim}}$  required for approaching the SW/S bound can be inferred  
322 in Fig. 5, which shows both the continuous-input–continuous-  
323 output memoryless channel’s (CCMC) capacity and the  
324 corresponding BPSK-based discrete-input–continuous-output  
325 memoryless channel’s (DCMC) capacity curve. For example,  
326 when aiming for a target throughput of  $\eta_{SW} = 0.366$  BPS for  
327 our DSTTCM-QPSK/BPSK scheme, the DCMC curve indi-

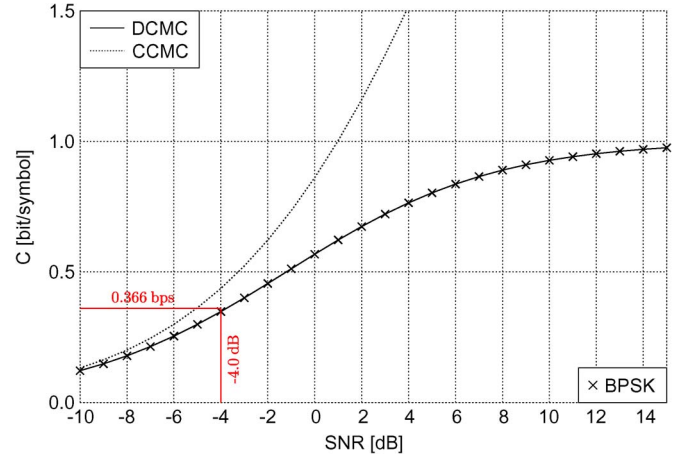


Fig. 5. DCMC and CCMC capacity curves, where the curves were computed based on [24].

331 cates the requirement of a minimum SNR of  $\Gamma_{\text{lim}} = -4$  dB, 328  
332 as shown in Fig. 5. Note that  $\Gamma_{\text{lim}}$  is represented with the aid of 329  
333 vertical lines in Fig. 4. 330

331 As expected, the proposed scheme benefits from the side  
332 information constituted by  $\{b_2\}$  while compressing the source  
333 sequence  $\{b_1\}$ . Note in Fig. 4 that all DSC schemes outperform  
334 the conventional TCM-QPSK benchmark scheme dispensing  
335 with joint decoding, which is labeled by the diamond markers,  
336 regardless of the correlation  $\rho$ , except for the very low correla-  
337 tion scenario<sup>5</sup> of  $\rho = 0.4$ . More explicitly, at a  $\text{BER} = 10^{-5}$ ,  
338 the proposed DSC has an SNR gain of 7.3, 6.2, and 3 dB  
339 for  $\rho = 0.86$ ,  $\rho = 0.8$ , and  $\rho = 0.6$ , respectively. However, as  
340 expected, with a low correlation value, the proposed scheme  
341 has an SNR loss of 1.3 dB, namely, when we have  $\rho = 0.4$ .  
342 Again, this is not unexpected because, for  $\rho < 0.5$ , the sources  
343 may be deemed to be uncorrelated; hence, they in fact provide  
344 misinformation misleading the joint decoder. It may be readily  
345 observed in Fig. 4 that, at  $\text{BER} = 10^{-5}$ , the scheme having  $\rho =$   
346 0.86 has the minimum distance with respect to the SW/S limit,  
347 i.e., we have  $\Gamma - \Gamma_{\text{lim}} = (-3.4) - (-4) = 0.6$  dB, whereas the  
348 scheme associated with  $\rho = 0.4$  has a distance of 1.7 dB from  
349 the limit. 349

350 The effect of the number of iterations between the TCM  
351 decoders in Fig. 3  $I$ , on the overall DSTTCM-QPSK/BPSK  
352 scheme’s performance, is shown in Fig. 6. It can be observed  
353 that doubling the number of iterations from  $I = 2$  to  $I = 4$   
354 will improve the scheme’s performance by 1.5 dB, whereas  
355 doubling the complexity further will only enhance the system’s  
356 performance by 0.5 dB. However, doubling the complexity  
357 beyond  $I = 8$  would not provide any further gain at the cost  
358 of increasing the decoding complexity; hence, we invoke eight  
359 iterations in our decoder. 359

360 The SW theoretical bound and the achievable rates obtained  
361 for the proposed DSTTCM-QPSK/BPSK schemes are shown,  
362 respectively, in Fig. 7. The rates achieved correspond to a  
363 BER of  $10^{-5}$ , and on average, the system’s throughput is only  
364 0.088 bits away from the bound shown in Fig. 4. Table I  
365 summarized the performance of the proposed scheme. 365

<sup>5</sup>The higher the crossover probability  $p_e$ , the lower the correlation between the two sources.

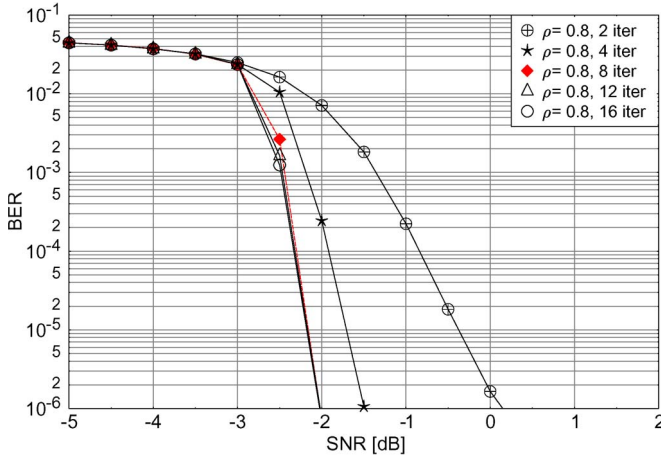


Fig. 6. BER versus SNR performance of the proposed DSTTCM-QPSK/BPSK scheme for the correlation parameter of  $\rho = \{0.8\}$  when transmitting over uncorrelated Rayleigh fading channels. The number of decoding iterations between the two TCM MAP decoders in Fig. 3 are  $I = \{2, 4, 8, 12, 16\}$ .

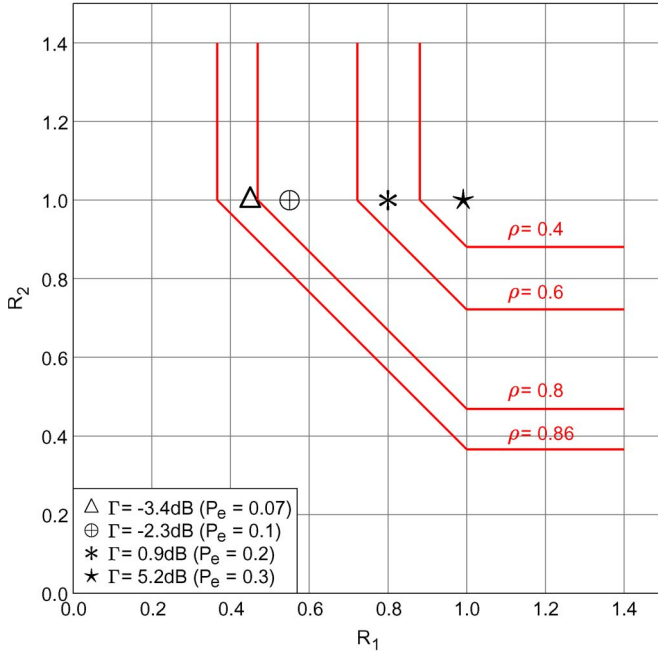


Fig. 7. Theoretical SW bound and the rates  $(R_1, R_2)$  achieved by the proposed DSTTCM-QPSK/BPSK scheme for different  $p_e$  values, where  $\Gamma$  denotes the SNR required for achieving a BER =  $10^{-5}$ .

TABLE I  
SYSTEM PERFORMANCE OF THE DSTTCM  
FOR SW CODING AT BER =  $10^{-5}$

$p_e$	$\rho$	$\eta_{SW}$	$\eta_{10^{-5}}$	SW-Gap (bits)	$\Gamma_{lim}$	$\Gamma$	Gap (dB)
0.07	0.86	0.366	0.41	0.084	-4.0	-3.4	0.6
0.1	0.80	0.469	0.55	0.081	-3.1	-2.3	0.80
0.2	0.60	0.722	0.8	0.078	0	0.9	0.90
0.3	0.40	0.881	1.0	0.108	3.5	5.2	1.7

366

#### IV. SIMULATION RESULTS

Our proposed design has also been extended to higher order modulation modes to conceive an adaptive scheme. Fig. 8 shows the BER performance of the different DSTTCM modes for  $\rho = 0.9$  and  $\rho = 0.8$  associated with crossover probabilities

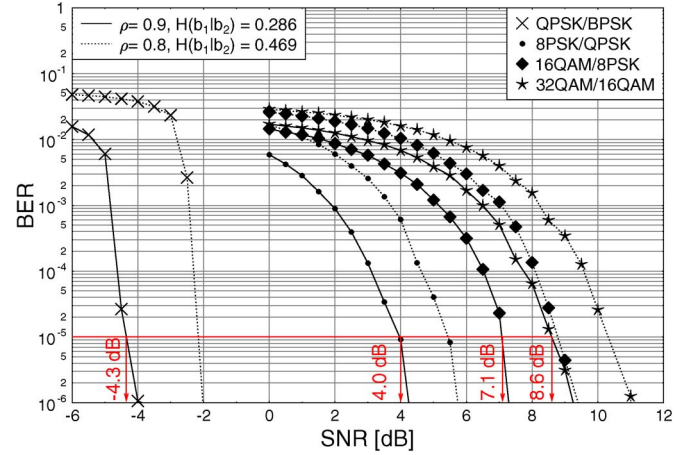


Fig. 8. BER versus SNR performance of the different TTCM modes, when using a block length of  $N_S = 12\,000$  symbols for  $\rho = 0.9$  and  $\rho = 0.86$  for transmission over uncorrelated Rayleigh fading channels.

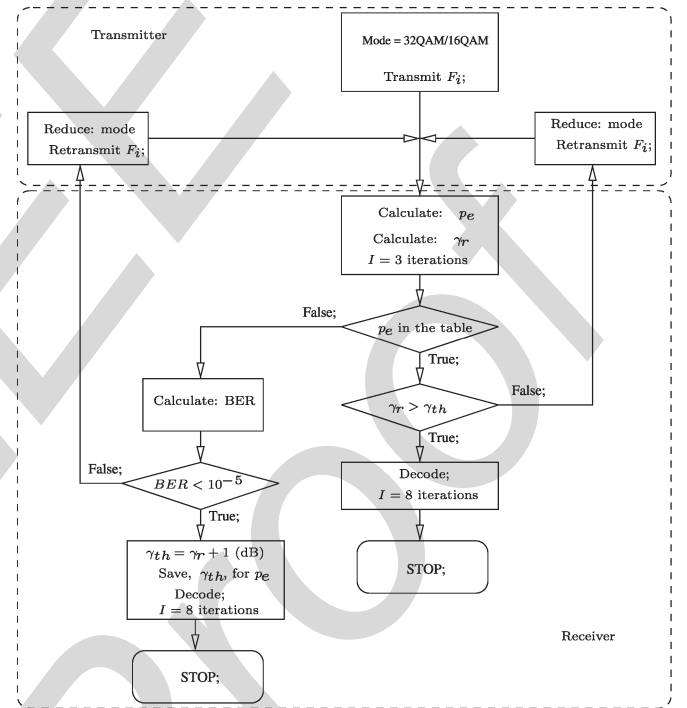


Fig. 9. Flowchart of the adaptive scheme.

of  $p_e = 0.05$  and  $p_e = 0.1$ , respectively, while using a block length of  $N_S = 12\,000$  symbols for all the modulation modes. A total of 10 000 blocks have been used in our simulations. The performance of the higher order modulation schemes shown in Fig. 8 suggests that the A-DSTTCM is readily applicable to SW coding. In each mode, we puncture the least significant bit of each coded symbol, which results in puncturing rates of  $R_p = \{2/1, 3/2, 4/3, 5/4\}$  for QPSK/BPSK, 8PSK/QPSK, 16QAM/8PSK, and 32QAM/16QAM, respectively. By comparing Figs. 4 and 8, observe that, as expected, the “QPSK/BPSK” scheme outperforms its counterparts in terms of its BER performance since it has a lower throughput.

The flowchart in Fig. 9 shows the adaptation process, where the current frame  $F_i$  will be transmitted first by the highest order 32QAM/16QAM modulation mode. Then, the crossover

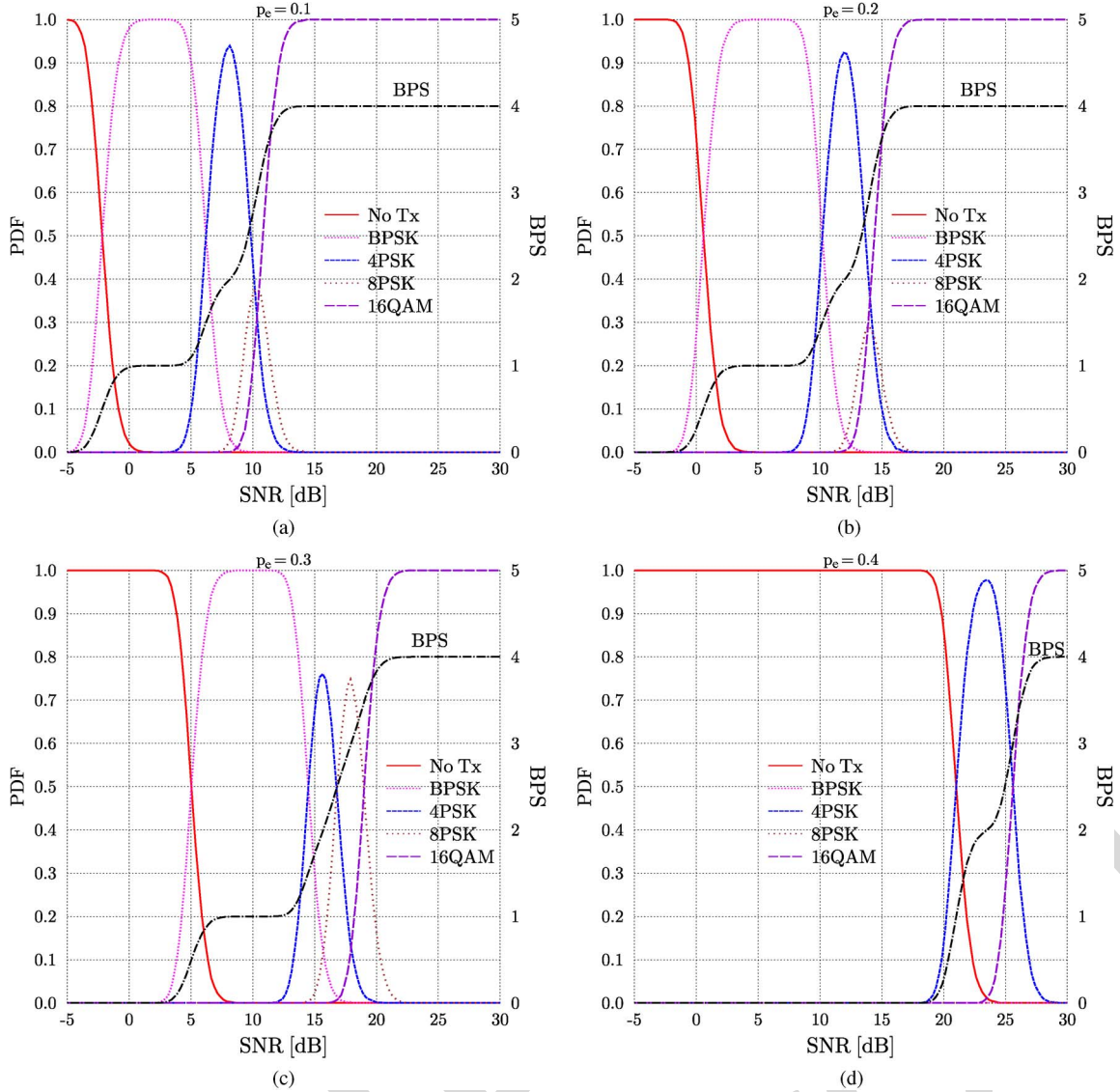


Fig. 10. PDF of all DSTTCM modes (left-hand vertical axis) versus the received SNR values and the corresponding BPS (right-hand vertical axis) versus the received SNR for  $\rho = \{0.8, 0.6, 0.4, 0.2\}$  when communicating over a Rayleigh fading channel. (a)  $\rho = 0.8$ . (b)  $\rho = 0.6$ . (c)  $\rho = 0.4$ . (d)  $\rho = 0.2$ .

386 probability  $p_e$ , which controls the correlation parameter of  $\rho =$   
 387  $1 - 2p_e$ , is estimated as [13]

$$\hat{p}_e = \frac{1}{N} \sum_{k=1}^N \Pr(b_1 = +1) \Pr(b_2 = -1) + \Pr(b_1 = -1) \Pr(b_2 = +1). \quad (11)$$

388 As few as three iterations are sufficient for estimating the  
 389 correlation parameter sufficiently accurately. Next, the near-  
 390 instantaneous SNR  $\gamma_r$  is calculated using the following:

$$\gamma_r = 10 \log_{10} (|h|^2 / N_0) \text{ [dB]}. \quad (12)$$

391 Then, the decoder will compare the estimated probability  $\hat{p}_e$  to  
 392 the prestored lookup table. The aim of this table is to reduce  
 393 the overall complexity of the adaptation process. As shown  
 394 in the flowchart, if  $p_e$  is not found in the table, the decoder  
 395 will estimate the BER of the received block, where the BER is  
 396 estimated after decoding by comparing the source sequence bits

$\{b_1\}$  with the decoded bits  $\{\hat{b}_1\}$ . Provided that the estimated  
 BER is below  $10^{-5}$ , the corresponding SNR  $\gamma_r$ , which are  
 indicated by the vertical arrows in Fig. 8 will be saved in the  
 lookup table as the threshold of  $\gamma_{th} = \gamma_r + 1$  (dB). Note that  
 the additional 1 dB and the three iterations used will reassure  
 that the performance of the adaptive scheme will remain below  
 a BER of  $10^{-5}$ . However, when we have  $\text{BER} < 10^{-5}$  or  $\gamma_r < 403$   
 $\gamma_{th}$ , a feedback acknowledgement will be transmitted to the  
 transmitter that triggers a reduction of the transmission mode  
 index/throughput. We opt to start with a higher rate mode to  
 reduce the number of feedback requests.<sup>6</sup> Hence, the overall  
 complexity and time required for performing this adaptive rate  
 adjustment process has been reduced. 409

Furthermore, the probability density function (pdf) of each  
 DSTTCM mode versus the average SNR is shown in Fig. 10,  
 along with the related BPS curves recorded for different

<sup>6</sup>An incremental mode-based adaptive scheme can be also implemented, subject to additional considerations.

413 correlation of  $\rho = \{0.8, 0.6, 0.4, 0.2\}$ , respectively. Naturally,  
 414 the choice of the specific DSTTCM modes is governed by  
 415 the particular near-instantaneous SNR experienced by the in-  
 416 dividual transmission frames at any specific average SNR value  
 417 in Fig. 10. The adaptive scheme maintains  $\text{BER} < 10^{-5}$ . It is  
 418 shown in Fig. 10 that, as the SNR increases, the higher order  
 419 DSTTCM modes are activated more often than the lower rate  
 420 ones. Consequently, the effective BPS throughput increases  
 421 smoothly with the SNR. It may be also observed from the figure  
 422 that, in the presence of a high correlation between the two  
 423 sources, such as  $\rho = 0.8$ , the no transmission mode has effec-  
 424 tively disappeared. However, for low correlations, the scheme  
 425 requires a higher SNR for achieving a nonzero throughput. The  
 426 adaptive procedure operated as follows. First, the BER of each  
 427 received block is estimated. If we have  $\text{BER} < 10^{-5}$ , then a  
 428 higher order modulation mode will be requested for the next  
 429 block.

## 430 V. CONCLUSION

431 In this paper, we have proposed a novel DSTTCM scheme for  
 432 a SW-distributed coding system. The proposed system outper-  
 433 formed the benchmark scheme dispensing with joint decoding  
 434 for a wide range of crossover probabilities. A modified symbol-  
 435 based MAP was proposed for exploiting the side information  
 436 available. The theoretical SW/S bounds were estimated, and  
 437 the proposed scheme was shown to operate within 0.7 dB  
 438 from it, for  $\rho = 0.86$  at a BER of  $10^{-5}$ . Our proposed scheme  
 439 operates within 0.088 bits of the maximum achievable rate  
 440 limit on average, which matches the best result reported in  
 441 the literature for similar systems while considering a realistic  
 442 Rayleigh fading channel model. Furthermore, a bandwidth-  
 443 efficient practical adaptive scheme was proposed based on a  
 444 range of adaptive modem modes for transmitting correlated  
 445 signals over uncorrelated Rayleigh fading channels. The trans-  
 446 mitter adapts its coding and modulation modes according to  
 447 both the short-term channel conditions and to the crossover  
 448 probabilities for ensuring that the BER remains below  $10^{-5}$ .

## 449 REFERENCES

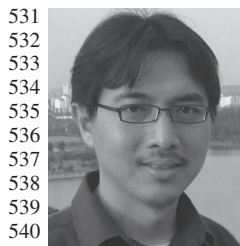
450 [1] Z. Xiong, A. Liveris, and S. Cheng, "Distributed source coding for sen-  
 451 sor networks," *IEEE Signal Process. Mag.*, vol. 21, no. 5, pp. 80–94,  
 452 Sep. 2004.  
 453 [2] A. Aaron and B. Girod, "Compression with side information using turbo  
 454 codes," in *Proc. DCC*, 2002, pp. 252–261.  
 455 [3] D. Slepian and J. K. Wolf, "Noiseless coding of correlated informa-  
 456 tion sources," *IEEE Trans. Inf. Theory*, vol. IT-19, no. 4, pp. 471–480,  
 457 Jul. 1973.  
 458 [4] B. Girod, A. Aaron, S. Rane, and D. Rebollo-Monedero, "Distributed  
 459 video coding," *Proc. IEEE*, vol. 93, no. 1, pp. 71–83, Jan. 2005.  
 460 [5] S. Draper, A. Khisti, E. Martinian, A. Vetro, and J. Yedidia, "Using  
 461 distributed source coding to secure fingerprint biometrics," in *Proc. IEEE*  
 462 *ICASSP*, Apr. 2007, vol. 2, pp. II-129–II-132.  
 463 [6] S. Pradhan and K. Ramchandran, "Distributed source coding using syn-  
 464 dromes (DISCUS): Design and construction," *IEEE Trans. Inf. Theory*,  
 465 vol. 49, no. 3, pp. 626–643, Mar. 2003.  
 466 [7] J. Garcia-Frias and Z. Xiong, "Distributed source and joint source-channel  
 467 coding: from theory to practice," in *Proc. IEEE ICASSP*, Mar. 2005,  
 468 vol. 5, pp. 1093–1096.  
 469 [8] J. Bajcsy and P. Mitran, "Coding for the Slepian–Wolf problem with  
 470 turbo codes," in *Proc. IEEE Global Telecommun. Conf.*, 2001, vol. 2,  
 471 pp. 1400–1404.

[9] J. Garcia-Frias, "Compression of correlated binary sources using turbo  
 472 codes," *IEEE Commun. Lett.*, vol. 5, no. 10, pp. 417–419, Oct. 2001. 473  
 [10] D. Varodayan, A. Aaron, and B. Girod, "Rate-adaptive codes for dis-  
 474 tributed source coding," *Elsevier Signal Process.*, vol. 86, no. 11, 475  
 pp. 3123–3130, Nov. 2006. 476  
 [11] A. Liveris, Z. Xiong, and C. Georghiadis, "Compression of binary sources  
 477 with side information at the decoder using LDPC codes," *IEEE Commun.*  
 478 *Lett.*, vol. 6, no. 10, pp. 440–442, Oct. 2002. 479  
 [12] M. Sartipi and F. Fekri, "Distributed source coding using short to mod-  
 480 erate length rate-compatible LDPC codes: The entire slepian-wolf rate  
 481 region," *IEEE Trans. Commun.*, vol. 56, no. 3, pp. 400–411, Mar. 2008. 482  
 [13] J. Garcia-Frias and Y. Zhao, "Near-Shannon/Slepian–Wolf performance  
 483 for unknown correlated sources over AWGN channels," *IEEE Trans.*  
 484 *Commun.*, vol. 53, no. 4, pp. 555–559, Apr. 2005. 485  
 [14] Y. Zhao, W. Zhong, and J. Garcia-Frias, "Transmission of correlated  
 486 senders over a Rayleigh fading multiple access channel," *Elsevier Signal*  
 487 *Process.*, vol. 86, no. 11, pp. 3150–3159, Apr. 2006. 488  
 [15] J. Del Ser, P. Crespo, and A. Munoz, "Joint source-channel decoding  
 489 of correlated sources over ISI channels," in *Proc. IEEE VTC Spring*,  
 490 Jun. 2005, vol. 1, pp. 625–629. 491  
 [16] K. Anwar and T. Matsumoto, "Iterative spatial demapping for two corre-  
 492 lated sources with power control over fading MAC," in *Proc. IEEE VTC*  
 493 *Spring*, May 2012, pp. 1–7. 494  
 [17] L. Hanzo, T. H. Liew, B. L. Yeap, and S. X. Ng, *Turbo Coding, Turbo*  
 495 *Equalisation and Space-Time Coding: EXIT-Chart Aided Near-Capacity*  
 496 *Designs for Wireless Channels*. Hoboken, NJ, USA: Wiley, 2010. 497  
 [18] D. Varodayan, Y.-C. Lin, and B. Girod, "Adaptive distributed source  
 498 coding," *IEEE Trans. Image Process.*, vol. 21, no. 5, pp. 2630–2640,  
 499 May 2012. 500  
 [19] A. Roumy, K. Lajnef, and C. Guillemot, "Rate-adaptive turbo-  
 501 syndrome scheme for slepian-wolf coding," in *Proc. ACSSC*, Nov. 2007,  
 502 pp. 545–549. 503  
 [20] X. Lv, R. Liu, and R. Wang, "A novel rate-adaptive distributed source  
 504 coding scheme using polar codes," *IEEE Commun. Lett.*, vol. 17, no. 1,  
 505 pp. 143–146, Jan. 2013. 506  
 [21] L. Cui, S. Wang, S. Cheng, and M. Yeary, "Adaptive binary slepian-wolf  
 507 decoding using particle based belief propagation," *IEEE Trans. Commun.*,  
 508 vol. 59, no. 9, pp. 2337–2342, Sep. 2011. 509  
 [22] P. Robertson and T. Wörz, "Bandwidth-efficient turbo trellis-coded mod-  
 510 ulation using punctured component codes," *IEEE J. Sel. Areas Commun.*,  
 511 vol. 16, no. 2, pp. 206–218, Feb. 1998. 512  
 [23] V. Toto-Zaraso, A. Roumy, and C. Guillemot, "Rate-adaptive codes for  
 513 the entire slepian-wolf region and arbitrarily correlated sources," in *Proc.*  
 514 *IEEE ICASSP*, Apr. 2008, pp. 2965–2968. 515  
 [24] S. X. Ng and L. Hanzo, "On the MIMO channel capacity of multi-  
 516 dimensional signal sets," *IEEE Trans. Veh. Technol.*, vol. 55, no. 2,  
 517 pp. 528–536, Mar. 2006. 518



**Abdulah Jeza Aljohani** received the B.S. degree 519  
 (with honors) in electronics and communication en- 520  
 gineering from King Abdulaziz University, Jeddah, 521  
 Saudi Arabia, in 2006 and the M.Sc. degree (with 522  
 distinction) in wireless communications from the 523  
 University of Southampton, Southampton, U.K., in 524  
 2009. He is currently working toward the Ph.D. 525  
 degree with the Communications, Signal Processing, 526  
 and Control Group, School of Electronics and Com- 527  
 puter Science, University of Southampton. 528

His current research interests include joint source/ 529  
 channel coding and distributed source coding. 530



**Soon Xin Ng** (S'99–M'03–SM'08) received the B.Eng. degree (with first-class honors) in electronics engineering and the Ph.D. degree in wireless communications from the University of Southampton, Southampton, U.K., in 1999 and 2002, respectively.

From 2003 to 2006, he was a Postdoctoral Research Fellow working on collaborative European research projects known as SCOUT, NEWCOM, and PHOENIX. Since August 2006, he has been with the School of Electronics and Computer Science, University of Southampton, where he is currently a

Senior Lecturer. He is involved in the OPTIMIX and CONCERTO European projects, as well as the IU-ATC and UC4G projects. He is the author of over 150 papers and the coauthor of two John Wiley/IEEE Press books. His research interests include adaptive coded modulation, coded modulation, channel coding, space–time coding, joint source and channel coding, iterative detection, orthogonal frequency-division multiplexing, multiple-input–multiple-output systems, cooperative communications, distributed coding, quantum error-correcting codes, and joint wireless-and-optical-fiber communications.

Dr. Ng is a Chartered Engineer and a Fellow of the Higher Education Academy in the U.K.



**Lajos Hanzo** (F'08) received the M.S. degree in electronics, the D.Sc. degree, and the Doctor Honoris Causa degree from the Technical University of Budapest, Budapest, Hungary, in 1976, 1983, and 2009, respectively.

During his 37-year career in telecommunications, he has held various research and academic posts in Hungary, Germany, and the U.K. From 2008 to 2012, he was a Chaired Professor with Tsinghua University, Beijing, China. Since 1986, he has been with the School of Electronics and Computer Science, University of Southampton, Southampton, U.K., where he is currently the Chair

of telecommunications. He is the coauthor of 20 John Wiley/IEEE Press books on mobile radio communications, totalling in excess of 10 000 pages, and the author of more than 1300 research entries at IEEE Xplore. He has successfully supervised more than 80 Ph.D. students. He is an enthusiastic supporter of industrial and academic liaison, and he offers a range of industrial courses. Currently, he is directing a 100-strong academic research team, working on a range of research projects in the field of wireless multimedia communications sponsored by industry, the Engineering and Physical Sciences Research Council U.K., the European Research Council's Advanced Fellow Grant, and the Royal Society's Wolfson Research Merit Award. His research is funded by the European Research Council's Senior Research Fellow Grant. For further information on research in progress and associated publications, see (<http://www-mobile.ecs.soton.ac.uk>). He has 17 000 + citations.

Dr. Hanzo is a Fellow of the Royal Academy of Engineering, the Institution of Engineering and Technology, and the European Association for Signal Processing. He has served both as a Technical Program Committee and General Chair of IEEE conferences, has presented keynote lectures, and has been awarded a number of distinctions. He is also a Governor of the IEEE Vehicular Technology Society.

IEEE  
Proof

AUTHOR QUERY

NO QUERY.

IEEE  
Proof

# TTCM-Aided Rate-Adaptive Distributed Source Coding for Rayleigh Fading Channels

Abdulah Jeza Aljohani, Soon Xin Ng, *Senior Member, IEEE*, and Lajos Hanzo, *Fellow, IEEE*

**Abstract**—Adaptive turbo-trellis-coded modulation (TTCM)-aided asymmetric distributed source coding (DSC) is proposed, where two correlated sources are transmitted to a destination node. The first source sequence is TTCM encoded and is further compressed before it is transmitted through a Rayleigh fading channel, whereas the second source signal is assumed to be perfectly decoded and, hence, to be flawlessly shown at the destination for exploitation as side information for improving the decoding performance of the first source. The proposed scheme is capable of reliable communications within 0.80 dB of the Slepian–Wolf/Shannon (SW/S) theoretical limit at a bit error rate (BER) of  $10^{-5}$ . Furthermore, its encoder is capable of accommodating time-variant short-term correlation between the two sources.

**Index Terms**—Distributed source coding (DSC), joint source-channel coding, Slepian–Wolf (SW) coding, Turbo-trellis-coded modulation (TTCM).

## I. INTRODUCTION

DISTRIBUTED source coding (DSC) [1] refers to the problem of compressing several physically separated, but correlated sources, where the receiver can perform joint decoding of both encoded signals. The schematic of asymmetric DSC [2] is shown in Fig. 1, where source sequence  $\{b_1\}$  is compressed before its transmission, whereas the correlated source signal  $\{b_2\}$  is assumed to be available at the decoder but not at the source  $\{b_1\}$ . More explicitly, the encoder has to compress  $\{b_1\}$  without knowing  $\{b_2\}$ , yet the decoder is capable of exploiting the knowledge of  $\{b_2\}$  for recovering  $\{b_1\}$ .

More explicitly, the Slepian–Wolf (SW) [3] coding theorem specifies the achievable rate regions of the compressed correlated sources  $\{b_1\}$  and  $\{b_2\}$  for transmission to a joint decoder as  $R_1 \geq H(b_1|b_2)$ ,  $R_2 \geq H(b_2|b_1)$ , and  $R_1 + R_2 \geq H(b_1, b_2)$ , where  $H(b_1|b_2)$  and  $H(b_1, b_2)$  denote the conditional entropy and joint entropy, respectively. Remarkably, this bound is identical, regardless whether joint encoding or joint decoding is used, i.e., regardless of where the joint processing takes

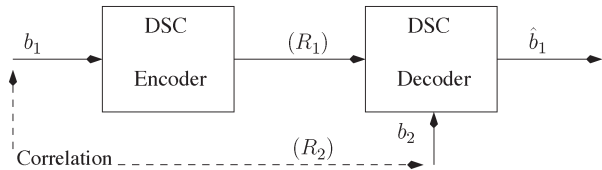


Fig. 1. Schematic of the asymmetric DSC.

place. This is quite convenient for exploiting the correlation of sources, which are distant from each other with the aid of joint processing at the receiver. This would facilitate for example the efficient joint decoding of correlated camera-phone-video sequences at the base station, namely, sequences, which portray the same scene from different angles.

This promising theoretical result has led to an increasing interest in a variety of applications, such as sensor networks [1], robust wireless video transmission [4], and compression of secure biometric data [5], where exchanging information between source nodes is not possible or not practical. Applying DSC techniques in wireless sensor networks, for example, has led to a new processing paradigm, where the potential computational complexity has been moved from the battery-limited sources to the central decoder connected to the mains supply.

As a consequence, the critical power constraint, which directly predetermines the life span of the wireless node, is fulfilled [1]. The first practical DSC technique was proposed in [6], where both sources  $\{b_1\}$  and  $\{b_2\}$  are assumed to be emitting equiprobable codewords, but they exhibit a difference because  $\{b_2\}$  is known only to the joint decoder but not to the encoder of  $\{b_1\}$ . Naturally, this assumption does not preclude that the codewords of  $\{b_2\}$  actually received from a remote source, but they must be first perfectly recovered in isolation before they may be used by the joint decoder for recovering  $\{b_1\}$ . Then, the codewords of both sources are grouped in cosets, where the members of each coset are separated by the maximum possible Hamming distance. Given  $\{b_2\}$  at the receiver, it is sufficient to transmit the index of the specific coset hosting the codewords of  $\{b_1\}$ . The decoder then estimates the transmitted codeword by choosing the one that is closest to the side information constituted by  $\{b_2\}$  of a given coset in terms of the Hamming distance.

The idea of using channel coding techniques<sup>1</sup> has enabled practical solutions to be developed. Practical Slepian–Wolf

Manuscript received July 8, 2013; revised September 30, 2013; accepted October 1, 2013. This work was supported in part by the Ministry of Higher Education of Saudi Arabia, by the European Union's Seventh Framework Programme through the CONCERTO Project under Grant 288502, by the Research Councils U.K. through the India–U.K. Advanced Technology Centre, by the European Research Council under an Advanced Fellow Grant, and by the Royal Society under the Wolfson Research Merit Award. The review of this paper was coordinated by Dr. E. K. S. Au.

The authors are with the Communications, Signal Processing, and Control Research Group, School of Electronics and Computer Science, University of Southampton, Southampton SO17 1BJ, U.K. (e-mail: ajra1c09@ecs.soton.ac.uk; sxn@ecs.soton.ac.uk; lh@ecs.soton.ac.uk).

Color versions of one or more of the figures in this paper are available online at <http://ieeexplore.ieee.org>.

Digital Object Identifier 10.1109/TVT.2013.2285020

<sup>1</sup>Since the correlation between the sources may be interpreted as the ameliorating effect of a “virtual” channel, a good channel code having, for example, a maximum minimum Hamming distance will be a good SW code [7].

76 schemes using turbo codes (TCs) were proposed for example  
 77 in [2], [8], and [9], whereas low-density parity-check (LDPC)  
 78 codes were considered in [10]–[12]. However, finding the best  
 79 code for approaching the Slepian–Wolf/Shannon (SW/S) limit  
 80 was not considered in [2], [8], and [9]. Later, a so-called “super”  
 81 TC was proposed in [13], aiming for approaching the SW/S  
 82 limit, when communicating over additive white Gaussian noise  
 83 (AWGN) channels. However, the scheme proposed in [13] for  
 84 an AWGN channel suffers from an error floor when communi-  
 85 cating over Rayleigh fading channels that makes the system less  
 86 suitable for wireless applications. A modified LDPC code was  
 87 proposed in [14] for mitigating the error floor, but nonetheless,  
 88 a high error floor persists when the correlation between the  
 89 sources is low. A joint turbo equalizer and decoder scheme  
 90 was proposed for asymmetric DSC in [15], whereas an iterative  
 91 joint turbo equalizer and decoder scheme was conceived for  
 92 transmission over a multipath Rayleigh fading multiple-access  
 93 channel in [16]. Both schemes have achieved a near-SW/S  
 94 performance, albeit at high joint decoding complexity. More  
 95 specifically, 35 iterations were invoked between the decoder  
 96 components in [15], whereas as many as 350 iterations were  
 97 required in [16] for attaining a near-SW/S performance. By  
 98 contrast, we only invoke eight turbo iterations in our TTCM  
 99 decoder, where both constituent decoders have comparable  
 100 complexity [17].

101 Furthermore, in practice, the short-term correlation among  
 102 the sources might be time variant; hence, adaptive-rate schemes  
 103 have to be considered, where the code rate is controlled via  
 104 a feedback channel. More specifically, if the bit error rate  
 105 (BER) evaluated after decoding exceeds a given threshold,  
 106 more syndromes (or parity bits if parity puncturing is used)  
 107 will be requested from the transmitter. A pair of innovative  
 108 adaptive-rate LDPC schemes was proposed in [18], whereas  
 109 adaptive-rate TCs were designed in [19]. In [18], the encoder  
 110 stored the syndromes and incrementally transmitted them to  
 111 the receiver, when the decoder failed to find the legitimate  
 112 codeword. Both papers considered an asymmetric DSC struc-  
 113 ture based on the puncturing of the syndrome generated by the  
 114 channel encoders, while stipulating the idealized simplifying  
 115 assumption of modeling the channel as the parallel combination  
 116 of a perfect channel and a binary symmetric channel (BSC).  
 117 More advanced adaptive-rate schemes considered the employ-  
 118 ment of a polar code [20] or efficient particle-based belief-  
 119 propagation-aided decoding [21] and density-evolution-based  
 120 decoding techniques [18].

121 Against this background, we propose a novel bandwidth-  
 122 efficient turbo-trellis-coded modulation (TTCM) scheme,  
 123 which combines the functions of coding and modulation for  
 124 conceiving a new DSCs system. TTCM [22] has a structure  
 125 similar to that of the family of binary TCs, where two identical  
 126 parallel-concatenated TCM schemes rather than conventional  
 127 codes are employed as component codes. The classic TTCM  
 128 design was outlined in [22], which is based on the search for  
 129 the best TCM component codes using the so-called “punctured”  
 130 minimal distance criterion, to approach the capacity of the  
 131 AWGN channel. The TTCM code advocated was designed to  
 132 improve the attainable throughput by considering the design of  
 133 error-correcting code and modulation where the parity bits are

absorbed in without any bandwidth expansion by increasing  
 the number of bits per modulated symbol. By contrast, all  
 separated channel codes, such as turbo or LDPC codes, impose  
 a bandwidth expansion, which is proportional to the code rate.  
 Furthermore, a novel adaptive-rate mechanism is conceived for  
 increasing the system’s effective throughput, while ensuring an  
 infinitesimally low BER. Hence, our new contributions are as  
 follows.

- We propose a uniquely amalgamated DSC and TTCM (DSTTCM) scheme for SW coding, which is capable of attaining a near-SW/S performance for a wide range of source correlation values. Our new scheme exhibits no error floor,<sup>2</sup> despite its low complexity. Furthermore, a carefully constructed modified symbol-based maximum *a posteriori* (MAP) algorithm is conceived for exploiting the side information available at the decoder. Additionally, we eliminate the aforementioned idealized simplifying assumptions exploited in the prior literature [18], [19], [23], and consider more realistic uncorrelated Rayleigh fading channels and BSCs.
- Furthermore, adaptive DSTTCM (A-DSTTCM) is proposed for accommodating the near-instantaneously time-varying nature of the wireless channel and the short-term correlation fluctuations among the sources. More explicitly, the system adapts its parameters according to both the channel quality and the correlation  $\rho$  of the sources,<sup>3</sup> while maintaining a given target BER.

The remainder of this paper is organized as follows. The proposed system model is described in Section II. The proposed scheme is designed in Section III. Section IV discusses our results. Finally, our conclusions are offered in Section V.

## II. SYSTEM MODEL

The asymmetric DSC scenario in Fig. 1 was considered here, where sequence  $\{b_2\}$  is transmitted at the rate of  $R_2 = H(b_2)$ , which is typically referred to as “side information” in most contributions [2], [8]; again, however, it can be also interpreted as another desired source signal, which was perfectly recovered. Sequence  $\{b_2\}$  can be also transmitted through an independent Rayleigh-fading channel, in which case, a similar encoder structure to that of the first source  $\{b_1\}$  has to be implemented. The problem in this scenario may be considered a symmetric DSC one. Symmetric DSC compression was discussed, for example, in [13], [14], and [16], but due to space limitations, it is beyond the scope of this paper.

Furthermore, crossover probability  $p_e$  used for modeling correlation parameter  $\rho$  may be assumed to be the overall probability of error, which is denoted as  $p_{e_1}$  and  $p_{e_2}$ . More explicitly, the error between the two sources is denoted by  $p_{e_1}$  and  $p_{e_2}$  which characterizes the transmission error between the second source and the destination. Thus, in this scenario, the overall error obeys  $p_e \leq p_{e_1} + p_{e_2}$ . The correlated sequence  $\{b_1\}$  is then compressed for approaching the Slepian–Wolf bound to a

<sup>2</sup>As documented in Fig. 4, no error floor is observed at above BER level of  $10^{-6}$ ; hence, our scheme is evidently suitable for wireless applications.

<sup>3</sup> $\rho$  is expressed using a crossover probability  $p_e$  as  $\rho = 1 - 2p_e$ .

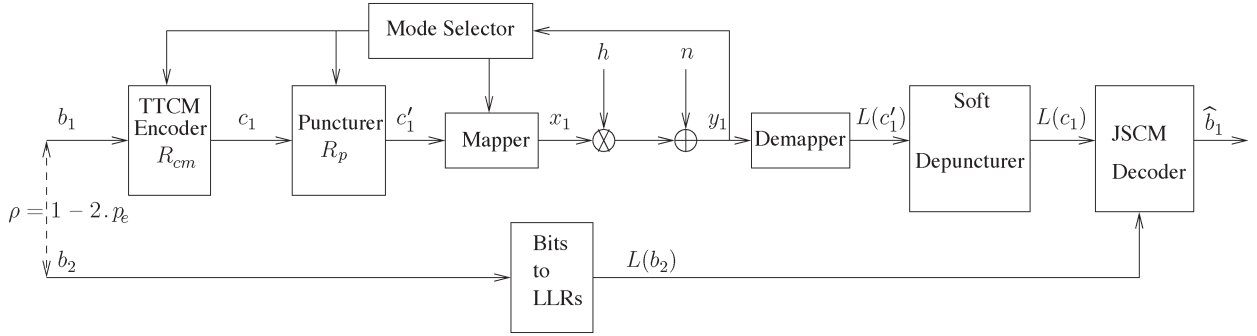


Fig. 2. Block diagram of the A-DSTTCM system communicating over Rayleigh fading channels. Sources  $\{b_1\}$  and  $\{b_2\}$  are assumed to be correlated, i.e., we have  $H(b_1 | b_2) \neq H(b_1)$ , and  $L(\cdot)$  denotes the LLRs.

186 rate of  $R_1 = H(b_1|b_2)$  to achieve the overall rate of  $H(b_1, b_2)$ .  
 187 Typically, the BSC is used for modeling the correlation between  
 188 the two source sequences  $\{b_1\} = \{b_1^1, b_1^2, \dots, b_1^i, \dots, b_1^N\}$  and  
 189  $\{b_2\} = \{b_2^1, b_2^2, \dots, b_2^i, \dots, b_2^N\}$ , where  $N$  is the length of each  
 190 source block.

191 For example, when  $\{b_1\}$  and  $\{b_2\}$  have a correlation of  
 192  $\rho = 0.9$  given the perfect knowledge of  $\{b_2\}$ ,  $\{b_1\}$  may be in-  
 193 terpreted as the output signal of BSC, which was contaminated  
 194 by the bit-flipping error events occurring with a probability  
 195 of  $p_e$ . Source sequence  $\{b_1\}$  is generated by an equiprobable  
 196 binary symmetric independent identically distributed (i.i.d.)  
 197 source, whereas  $\{b_2\}$  can be defined as  $b_1^i = b_2^i \oplus e_i$ , where  $\oplus$   
 198 is the modulo-2 addition operation, and  $e_i$  is an independent  
 199 binary random variable assuming the logical value of 1 with  
 200 a crossover probability of  $p_e$  and of 0 with a probability of  
 201  $(1 - p_e)$ . Both the random variables of  $b_1^i$  and  $b_2^i$  in the pair  
 202 of bit streams  $\{b_1\}$  and  $\{b_2\}$  may be assumed to be i.i.d. for  
 203 the bit index  $i$ ; hence, both sources emit equiprobable [16] bits.  
 204 Consequently, the entropy of each source is unity, which yields  
 205 conditional entropy of

$$\begin{aligned}
 H(p_e) &= H(b_1|b_2) \\
 &= \lim_{i \rightarrow \infty} \frac{1}{i} H((b_1^1, \dots, b_1^i, \dots, b_1^N) | (b_1^2, \dots, b_1^i, \dots, b_1^N))
 \end{aligned} \tag{1}$$

206 where  $H(p_e) = p_e \log_2(1/p_e) + (1 - p_e) \log_2(1/(1 - p_e))$  is  
 207 the entropy of the binary random variable, and  $e_i$  is used for  
 208 parametrizing the side information/ Therefore, the achievable  
 209 SW rate region is given by the following three inequalities [16]:

$$\begin{aligned}
 R_1 &\geq H(p_e) \\
 R_2 &\geq H(p_e) \\
 R_1 + R_2 &\geq 1 + H(p_e).
 \end{aligned} \tag{2}$$

210 Let us now embark on the design of a joint source-channel  
 211 (JSC) decoding scheme for minimizing the signal-to-noise  
 212 power ratio (SNR) required for approaching the SW/S bound,  
 213 while maintaining reliable communications. More explicitly,  
 214 let us define  $\text{SNR} = R_1 \cdot E_b/N_0$ , where  $E_b/N_0$  denotes the  
 215 energy per bit to noise power spectral density.

### A. Encoder

216

The block diagram of the proposed A-DSTTCM scheme con- 217  
 sidered for transmitting correlated sources is shown in Fig. 2, 218  
 where  $L(\cdot)$  denotes the log-likelihood ratios (LLRs) of the bits. 219  
 As shown in Fig. 2, the input sequence  $\{b_1\}$  is fed into a 220  
 TTCM encoder, which has a coding rate of  $R_{cm} = m/m + 1$  221  
 and invokes a  $2^{m+1}$ -level modulation scheme. The TTCM- 222  
 encoded bits are then punctured at a rate of  $R_p$ . The resultant bit 223  
 sequence  $\{c'_1\}$  is then mapped to the corresponding modulated 224  
 symbols  $\{x_1\}$  before their transmission over an uncorrelated 225  
 Rayleigh fading channel. The second bit sequence  $\{b_2\}$  will 226  
 be converted to the LLRs  $L(b_2) = L_e$ , which is then will be 227  
 exploited as side information. This conversion is necessary 228  
 because the joint decoder is a soft-decision-based one. These 229  
 LLRs are characterized by the aforementioned crossover prob- 230  
 ability  $p_e$  and can be estimated as 231

$$\begin{aligned}
 L(b_2|b_1) &= \ln \left[ \frac{\Pr(b_2 = +1|b_1)}{\Pr(b_2 = -1|b_1)} \right] \\
 &= \ln \left[ \frac{(1 - p_e) \Pr(b_1 = +1) + p_e \Pr(b_1 = -1)}{(1 - p_e) \Pr(b_1 = -1) + p_e \Pr(b_1 = +1)} \right].
 \end{aligned} \tag{3}$$

We assume that these LLRs are available at the destination 232  
 and to be exploited by the joint decoder, whereas  $p_e$  can be 233  
 estimated at the decoder using (11). 234

As an example, we use a rate  $R_{cm} = 1/2$  TTCM encoder 235  
 relying on a puncturer of rate  $R_p = 2/1$ , which punctures 236  
 one bit out of two encoded bits. We assume that all the 237  
 systematic bits are punctured, whereas all the parity bits are 238  
 transmitted to the decoder. Hence, the overall code rate is 239  
 $R_1 = R_{cm} \cdot R_p = 1$ . However, the parity bit sequence may be 240  
 also further punctured to achieve an increased compression 241  
 ratio. The resultant bits are then mapped to binary phase-shift 242  
 keying (BPSK) symbols, i.e., the modulation mode has been 243  
 changed from quadrature phase-shift keying (QPSK) to BPSK 244  
 (QPSK/BPSK). Thus, the corresponding effective throughput 245  
 is given by  $\eta = R_1 \cdot \log_2(2) = 1$  bits per symbol (BPS). Then, 246  
 the modulated symbol sequence  $\{x_1\}$  is transmitted over an 247  
 uncorrelated Rayleigh fading channel, and the received symbol 248  
 $y_1$  is given by 249

$$y_1 = hx_1 + n \tag{4}$$

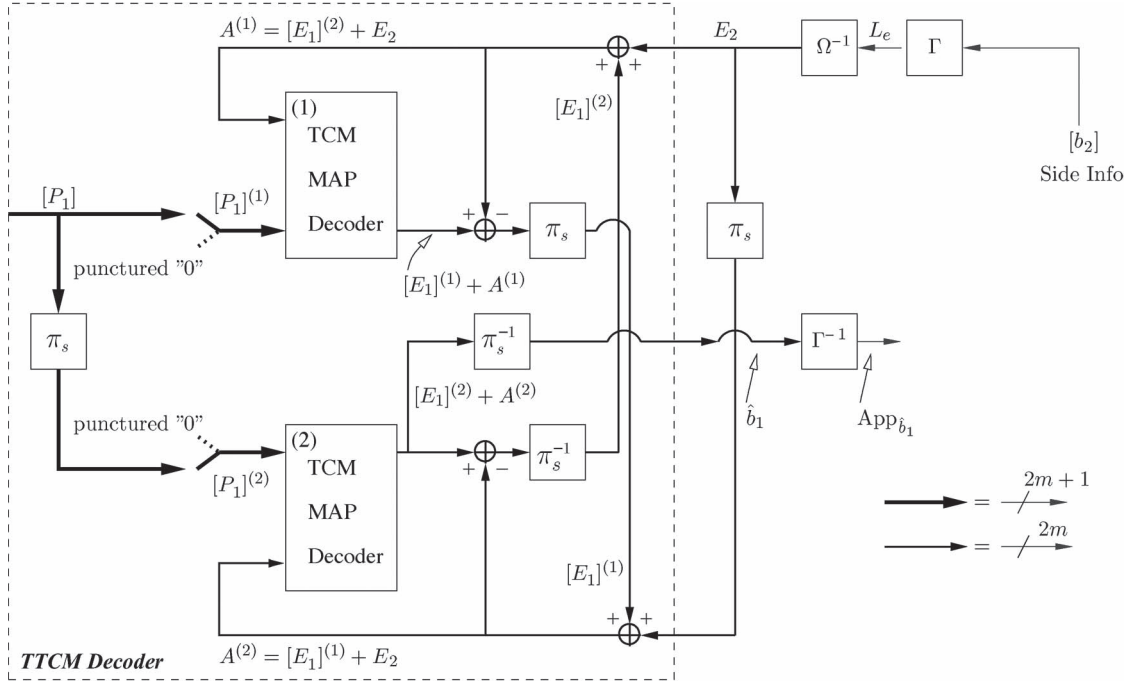


Fig. 3. Block diagram of the JSC-aided TTCM decoder conceived for our DSC system. Notations  $\pi_s$  and  $\pi_s^{-1}$  represent the symbol interleaver and deinterleaver, respectively, whereas  $\Gamma$  and  $\Gamma^{-1}$  denote the relevant symbol-to-LLR and LLR-to-symbol probability conversion.

250 where  $h$  is the fading coefficient of the channel, and  $n$  is the  
251 AWGN having a variance of  $N_0/2$  per dimension. The short-  
252 term average received SNR is given by

$$\text{SNR}_r = \frac{E\{|h|^2\}E\{|x_1|^2\}}{N_0} \quad (5)$$

253 where  $x_1$  represents the modulated symbols of source  $\{b_1\}$   
254 after puncturing. Furthermore, we have  $E\{|x_1|^2\} = 1$ , and  
255 the SNR of  $\gamma_r = 10 \log_{10}(|h|^2/N_0)$  [dB] is estimated for each  
256 received block. Note that  $\{b_2\}$  is related to  $\{b_1\}$  according  
257 to  $b_1^i = b_2^i \oplus e_i$ , as detailed in Section II. Diverse effective  
258 throughputs may be derived by changing  $R_{cm}$  and  $R_p$ ; hence,  
259 the proposed scheme exhibits substantial flexibility. In our  
260 A-DSTTCM scheme, the following modes are chosen at the  
261 encoder to ensure that  $\text{BER} < 10^{-5}$ :

- 262 • No transmission;
- 263 • DSTTCM-QPSK/BPSK;
- 264 • DSTTCM-8PSK/QPSK;
- 265 • DSTTCM-16-quadrature amplitude modulation (QAM)/  
266 8PSK;
- 267 • DSTTCM-32QAM/16QAM.

268 Thus, the effective throughput of our adaptive system as-  
269 sumes the values of  $\eta = \{0, 1, 2, 3, 4\}$  BPS.

### 270 B. Joint Source–Channel Decoder

271 Our JSC-decoding-aided DSTTCM scheme is shown in  
272 Fig. 3. Both TCM decoders invoke the symbol-based MAP  
273 algorithm [17] operating in the logarithmic domain. The TCM  
274 decoders are labeled with the round-bracketed indexes, whereas  
275 the notation  $P$ ,  $A$ , and  $E$  denote the logarithmic probabilities  
276 of the *a posteriori*, *a priori*, and *extrinsic* information, respec-  
277 tively, where  $L_e = L(b_2|b_1)$ . The  $2^{(m+1)}$ -ary  $P$  probabilities

associated with a specific  $(m+1)$ -bit TTCM-coded symbol 278  
 $\{c_1'\}$  are fed into the TTCM MAP decoder. A pair of signal 279  
components is generated by the constituent TCM decoders [17]; 280  
specifically, the *extrinsic* probability  $E$  is generated by each 281  
of the TCM decoders, whereas the *a priori* probability  $A$  is 282  
gleaned by each TCM decoder from the other one. Furthermore, 283  
as shown in Fig. 3, the additional *extrinsic* probability  $E_2$  284  
extracted from the side information  $\{b_2\}$  is also added to 285  
the *a priori* probability  $A$ , yielding  $A^{(1,2)} = [E_1]^{(2,1)} + E_2$ . 286  
Each of the constituent TCM blocks in Fig. 3 calculates the 287  
*a posteriori* probabilities using the forward and backward re- 288  
cursion methods.<sup>4</sup> 289

Upon recalling (4), we are now in the position to formulate 290  
the channel's transition metric as 291

$$\eta_i(\dot{s}, s) = \ln \left\{ \frac{1}{\pi N_0} e^{-|y_1 - h x_1|^2 / N_0} \right\}. \quad (6)$$

Then, both the backward and forward recursion methods of 292  
[17] are invoked for calculating  $\beta_{i-1}(\dot{s})$  and  $\alpha_i(s)$  as follows: 293

$$\alpha_i(s) = \max_{\dot{s}}^* \left( \alpha_{i-1}(\dot{s}) + \eta_i(\dot{s}, s) + A^{(1,2)} \right) \quad (7)$$

$$\beta_{i-1}(\dot{s}) = \max_s^* \left( \beta_i(s) + \eta_i(\dot{s}, s) + A^{(1,2)} \right) \quad (8)$$

where  $\max^*$  represents the Jacobian logarithm [17] evaluating 294  
all variables in the logarithmic domain, with  $(\dot{s}, s)$  denoting the 295  
transitions emerging from the previous state  $\dot{s}$  to the present 296  
state  $s$ . 297

<sup>4</sup>Detailed descriptions can be found in [17, Sec. 14.3]. Note that we illustrate the MAP process in the logarithmic domain to render it compatible with Fig. 3.

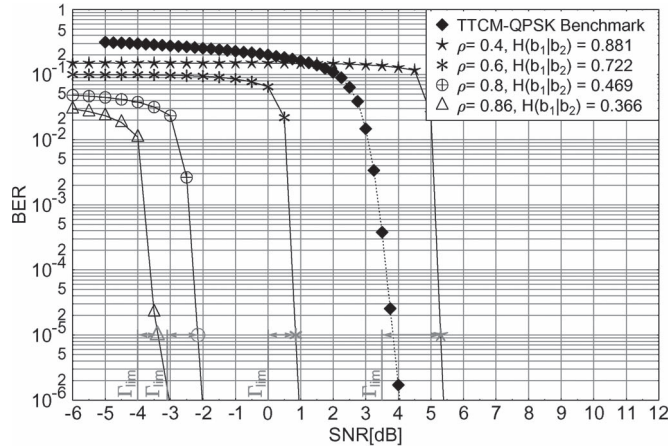


Fig. 4. BER versus SNR performance of the proposed DSTTCM-QPSK/BPSK scheme for correlation parameters of  $\rho = \{0.4, 0.6, 0.8, 0.86\}$  when transmitting over uncorrelated Rayleigh fading channels. The number of decoding iterations is  $I = 8$ .

### III. RATE REGION DESIGN AND ANALYSIS

The achieved rate region experienced in a noisy channel for both sources is given by [13], [16]:

$$\begin{aligned} H(b_1, b_2) &\leq \frac{C_1}{R_1} + \frac{C_2}{R_2} \\ &\leq \frac{1}{R_1} E\{\log_2(1 + \gamma_1)\} + \frac{1}{R_2} E\{\log_2(1 + \gamma_2)\} \end{aligned} \quad (9)$$

where  $C_1 = E\{\log_2(1 + \gamma_1)\}$  and  $C_2 = E\{\log_2(1 + \gamma_2)\}$  denote the ergodic channel capacities between each of the sources and the destination, whereas  $\gamma_1$  and  $\gamma_2$  denote the corresponding received SNRs. In our asymmetric system, we assume that  $\{b_2\}$  is transmitted at  $R_2 = H(b_2) = 1$ , whereas we aim for compressing  $\{b_1\}$  to its minimum rate, namely, to  $R_1 = H(b_1|b_2)$ . Then, based on (9), the effective throughput of our scheme for the  $\{b_1\}$  link can be expressed as  $\eta_{SW} = R_1 \cdot H(b_1|b_2)$ , whereas the SW/S bound is calculated as [15]

$$R_1 \cdot H(b_1|b_2) \leq C_1 \quad (10)$$

where  $C_1$  represents the ergodic capacity of the uncorrelated Rayleigh fading channel.

First we characterize the BER performance of our DSTTCM-QPSK/BPSK scheme employing a range of correlations  $\rho = \{0.4, 0.6, 0.8, 0.86\}$ . We opted for using 1/2-rate TTCM for encoding a block of  $N_S = 12\,000$  symbols, resulting in  $N_b = 24\,000$  bits before we remove all of the systematic bits from the TTCM-coded sequence with the aid of puncturing. The BER versus SNR performance of the proposed system is shown in Fig. 4. Note that the SNR can be calculated in decibels as  $\text{SNR}(\text{dB}) = E_b/N_0(\text{dB}) + 10 \log(R_1)$ . The minimum SNR  $\Gamma_{\text{lim}}$  required for approaching the SW/S bound can be inferred in Fig. 5, which shows both the continuous-input–continuous-output memoryless channel’s (CCMC) capacity and the corresponding BPSK-based discrete-input–continuous-output memoryless channel’s (DCMC) capacity curve. For example, when aiming for a target throughput of  $\eta_{SW} = 0.366$  BPS for our DSTTCM-QPSK/BPSK scheme, the DCMC curve indi-

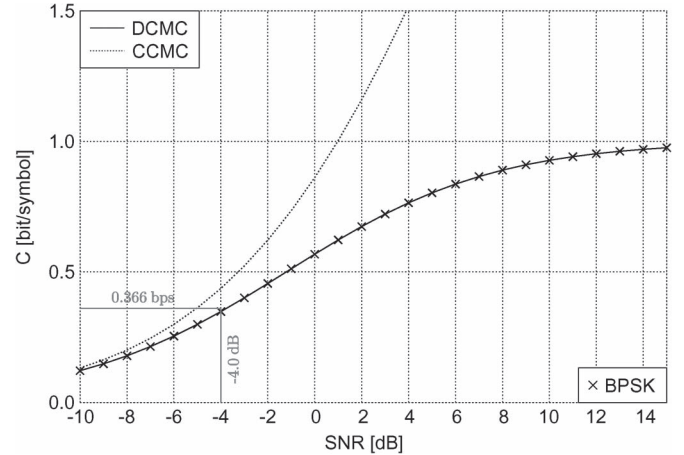


Fig. 5. DCMC and CCMC capacity curves, where the curves were computed based on [24].

icates the requirement of a minimum SNR of  $\Gamma_{\text{lim}} = -4$  dB, 328 as shown in Fig. 5. Note that  $\Gamma_{\text{lim}}$  is represented with the aid of 329 vertical lines in Fig. 4. 330

As expected, the proposed scheme benefits from the side 331 information constituted by  $\{b_2\}$  while compressing the source 332 sequence  $\{b_1\}$ . Note in Fig. 4 that all DSC schemes outperform 333 the conventional TTCM-QPSK benchmark scheme dispensing 334 with joint decoding, which is labeled by the diamond markers, 335 regardless of the correlation  $\rho$ , except for the very low correla- 336 tion scenario<sup>5</sup> of  $\rho = 0.4$ . More explicitly, at a BER =  $10^{-5}$ , 337 the proposed DSC has an SNR gain of 7.3, 6.2, and 3 dB 338 for  $\rho = 0.86$ ,  $\rho = 0.8$ , and  $\rho = 0.6$ , respectively. However, as 339 expected, with a low correlation value, the proposed scheme 340 has an SNR loss of 1.3 dB, namely, when we have  $\rho = 0.4$ . 341 Again, this is not unexpected because, for  $\rho < 0.5$ , the sources 342 may be deemed to be uncorrelated; hence, they in fact provide 343 misinformation misleading the joint decoder. It may be readily 344 observed in Fig. 4 that, at BER =  $10^{-5}$ , the scheme having  $\rho = 345$  0.86 has the minimum distance with respect to the SW/S limit, 346 i.e., we have  $\Gamma - \Gamma_{\text{lim}} = (-3.4) - (-4) = 0.6$  dB, whereas the 347 scheme associated with  $\rho = 0.4$  has a distance of 1.7 dB from 348 the limit. 349

The effect of the number of iterations between the TCM 350 decoders in Fig. 3  $I$ , on the overall DSTTCM-QPSK/BPSK 351 scheme’s performance, is shown in Fig. 6. It can be observed 352 that doubling the number of iterations from  $I = 2$  to  $I = 4$  353 will improve the scheme’s performance by 1.5 dB, whereas 354 doubling the complexity further will only enhance the system’s 355 performance by 0.5 dB. However, doubling the complexity 356 beyond  $I = 8$  would not provide any further gain at the cost 357 of increasing the decoding complexity; hence, we invoke eight 358 iterations in our decoder. 359

The SW theoretical bound and the achievable rates obtained 360 for the proposed DSTTCM-QPSK/BPSK schemes are shown, 361 respectively, in Fig. 7. The rates achieved correspond to a 362 BER of  $10^{-5}$ , and on average, the system’s throughput is only 363 0.088 bits away from the bound shown in Fig. 4. Table I 364 summarized the performance of the proposed scheme. 365

<sup>5</sup>The higher the crossover probability  $p_e$ , the lower the correlation between the two sources.

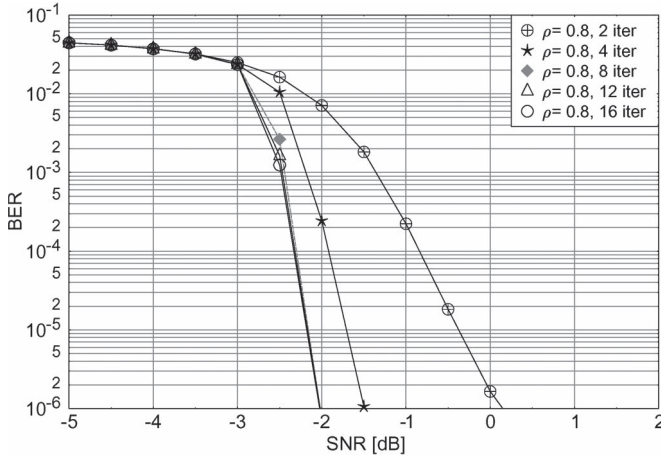


Fig. 6. BER versus SNR performance of the proposed DSTTCM-QPSK/BPSK scheme for the correlation parameter of  $\rho = \{0.8\}$  when transmitting over uncorrelated Rayleigh fading channels. The number of decoding iterations between the two TCM MAP decoders in Fig. 3 are  $I = \{2, 4, 8, 12, 16\}$ .

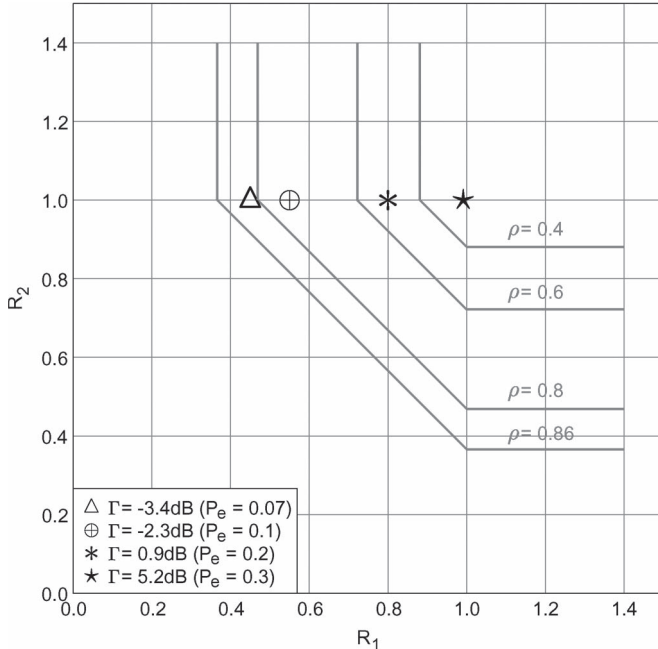


Fig. 7. Theoretical SW bound and the rates  $(R_1, R_2)$  achieved by the proposed DSTTCM-QPSK/BPSK scheme for different  $p_e$  values, where  $\Gamma$  denotes the SNR required for achieving a BER =  $10^{-5}$ .

TABLE I  
SYSTEM PERFORMANCE OF THE DSTTCM  
FOR SW CODING AT BER =  $10^{-5}$

$p_e$	$\rho$	$\eta_{SW}$	$\eta_{10^{-5}}$	SW-Gap (bits)	$\Gamma_{lim}$	$\Gamma$	Gap (dB)
0.07	0.86	0.366	0.41	0.084	-4.0	-3.4	0.6
0.1	0.80	0.469	0.55	0.081	-3.1	-2.3	0.80
0.2	0.60	0.722	0.8	0.078	0	0.9	0.90
0.3	0.40	0.881	1.0	0.108	3.5	5.2	1.7

366

#### IV. SIMULATION RESULTS

Our proposed design has also been extended to higher order modulation modes to conceive an adaptive scheme. Fig. 8 shows the BER performance of the different DSTTCM modes for  $\rho = 0.9$  and  $\rho = 0.8$  associated with crossover probabilities

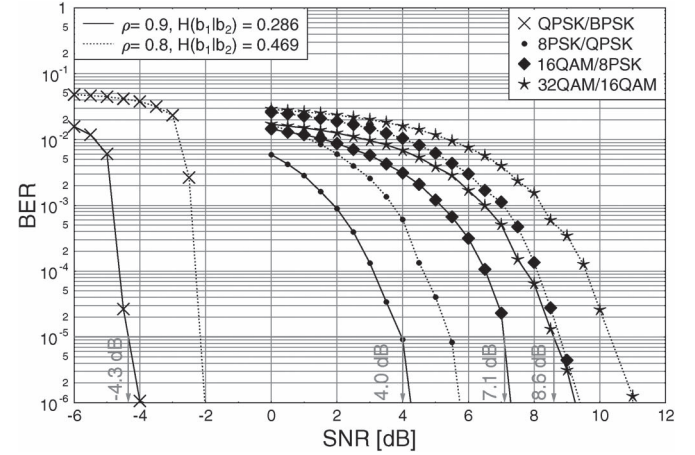


Fig. 8. BER versus SNR performance of the different TTCM modes, when using a block length of  $N_S = 12\,000$  symbols for  $\rho = 0.9$  and  $\rho = 0.86$  for transmission over uncorrelated Rayleigh fading channels.

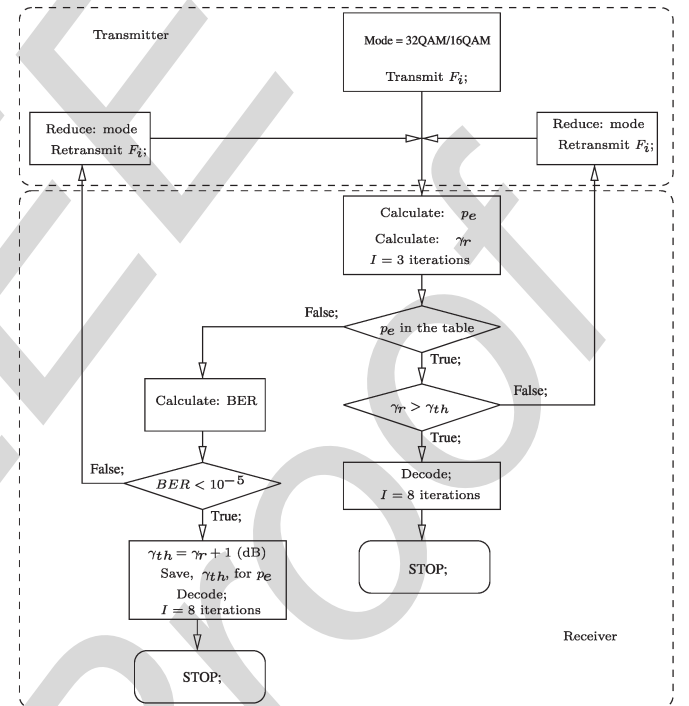


Fig. 9. Flowchart of the adaptive scheme.

of  $p_e = 0.05$  and  $p_e = 0.1$ , respectively, while using a block length of  $N_S = 12\,000$  symbols for all the modulation modes. A total of 10 000 blocks have been used in our simulations. The performance of the higher order modulation schemes shown in Fig. 8 suggests that the A-DSTTCM is readily applicable to SW coding. In each mode, we puncture the least significant bit of each coded symbol, which results in puncturing rates of  $R_p = \{2/1, 3/2, 4/3, 5/4\}$  for QPSK/BPSK, 8PSK/QPSK, 16QAM/8PSK, and 32QAM/16QAM, respectively. By comparing Figs. 4 and 8, observe that, as expected, the “QPSK/BPSK” scheme outperforms its counterparts in terms of its BER performance since it has a lower throughput.

The flowchart in Fig. 9 shows the adaptation process, where the current frame  $F_i$  will be transmitted first by the highest order 32QAM/16QAM modulation mode. Then, the crossover

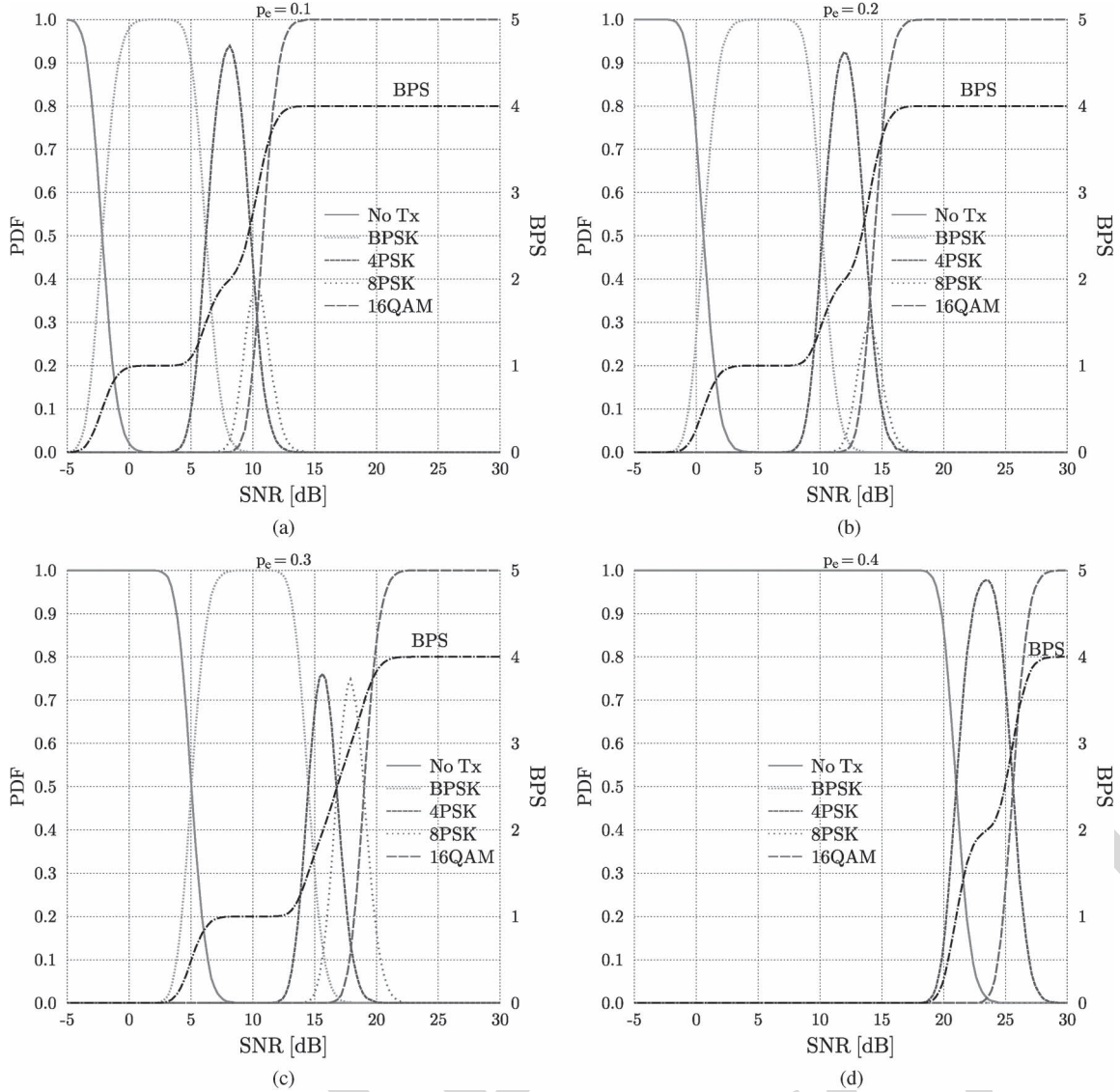


Fig. 10. PDF of all DSTTCM modes (left-hand vertical axis) versus the received SNR values and the corresponding BPS (right-hand vertical axis) versus the received SNR for  $\rho = \{0.8, 0.6, 0.4, 0.2\}$  when communicating over a Rayleigh fading channel. (a)  $\rho = 0.8$ . (b)  $\rho = 0.6$ . (c)  $\rho = 0.4$ . (d)  $\rho = 0.2$ .

386 probability  $p_e$ , which controls the correlation parameter of  $\rho =$   
 387  $1 - 2p_e$ , is estimated as [13]

$$\hat{p}_e = \frac{1}{N} \sum_{k=1}^N \Pr(b_1 = +1) \Pr(b_2 = -1) + \Pr(b_1 = -1) \Pr(b_2 = +1). \quad (11)$$

388 As few as three iterations are sufficient for estimating the  
 389 correlation parameter sufficiently accurately. Next, the near-  
 390 instantaneous SNR  $\gamma_r$  is calculated using the following:

$$\gamma_r = 10 \log_{10} (|h|^2 / N_0) \text{ [dB]}. \quad (12)$$

391 Then, the decoder will compare the estimated probability  $\hat{p}_e$  to  
 392 the prestored lookup table. The aim of this table is to reduce  
 393 the overall complexity of the adaptation process. As shown  
 394 in the flowchart, if  $p_e$  is not found in the table, the decoder  
 395 will estimate the BER of the received block, where the BER is  
 396 estimated after decoding by comparing the source sequence bits

$\{b_1\}$  with the decoded bits  $\{\hat{b}_1\}$ . Provided that the estimated  
 BER is below  $10^{-5}$ , the corresponding SNR  $\gamma_r$ , which are  
 indicated by the vertical arrows in Fig. 8 will be saved in the  
 lookup table as the threshold of  $\gamma_{th} = \gamma_r + 1$  (dB). Note that  
 the additional 1 dB and the three iterations used will reassure  
 that the performance of the adaptive scheme will remain below  
 a BER of  $10^{-5}$ . However, when we have  $\text{BER} < 10^{-5}$  or  $\gamma_r < 403$   
 $\gamma_{th}$ , a feedback acknowledgement will be transmitted to the  
 transmitter that triggers a reduction of the transmission mode  
 index/throughput. We opt to start with a higher rate mode to  
 reduce the number of feedback requests.<sup>6</sup> Hence, the overall  
 complexity and time required for performing this adaptive rate  
 adjustment process has been reduced. 409

Furthermore, the probability density function (pdf) of each  
 DSTTCM mode versus the average SNR is shown in Fig. 10,  
 along with the related BPS curves recorded for different

<sup>6</sup>An incremental mode-based adaptive scheme can be also implemented,  
 subject to additional considerations.

413 correlation of  $\rho = \{0.8, 0.6, 0.4, 0.2\}$ , respectively. Naturally,  
 414 the choice of the specific DSTTCM modes is governed by  
 415 the particular near-instantaneous SNR experienced by the in-  
 416 dividual transmission frames at any specific average SNR value  
 417 in Fig. 10. The adaptive scheme maintains  $\text{BER} < 10^{-5}$ . It is  
 418 shown in Fig. 10 that, as the SNR increases, the higher order  
 419 DSTTCM modes are activated more often than the lower rate  
 420 ones. Consequently, the effective BPS throughput increases  
 421 smoothly with the SNR. It may be also observed from the figure  
 422 that, in the presence of a high correlation between the two  
 423 sources, such as  $\rho = 0.8$ , the no transmission mode has effec-  
 424 tively disappeared. However, for low correlations, the scheme  
 425 requires a higher SNR for achieving a nonzero throughput. The  
 426 adaptive procedure operated as follows. First, the BER of each  
 427 received block is estimated. If we have  $\text{BER} < 10^{-5}$ , then a  
 428 higher order modulation mode will be requested for the next  
 429 block.

## 430 V. CONCLUSION

431 In this paper, we have proposed a novel DSTTCM scheme for  
 432 a SW-distributed coding system. The proposed system outper-  
 433 formed the benchmark scheme dispensing with joint decoding  
 434 for a wide range of crossover probabilities. A modified symbol-  
 435 based MAP was proposed for exploiting the side information  
 436 available. The theoretical SW/S bounds were estimated, and  
 437 the proposed scheme was shown to operate within 0.7 dB  
 438 from it, for  $\rho = 0.86$  at a BER of  $10^{-5}$ . Our proposed scheme  
 439 operates within 0.088 bits of the maximum achievable rate  
 440 limit on average, which matches the best result reported in  
 441 the literature for similar systems while considering a realistic  
 442 Rayleigh fading channel model. Furthermore, a bandwidth-  
 443 efficient practical adaptive scheme was proposed based on a  
 444 range of adaptive modem modes for transmitting correlated  
 445 signals over uncorrelated Rayleigh fading channels. The trans-  
 446 mitter adapts its coding and modulation modes according to  
 447 both the short-term channel conditions and to the crossover  
 448 probabilities for ensuring that the BER remains below  $10^{-5}$ .

## 449 REFERENCES

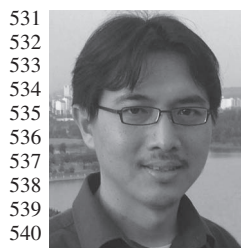
450 [1] Z. Xiong, A. Liveris, and S. Cheng, "Distributed source coding for sen-  
 451 sor networks," *IEEE Signal Process. Mag.*, vol. 21, no. 5, pp. 80–94,  
 452 Sep. 2004.  
 453 [2] A. Aaron and B. Girod, "Compression with side information using turbo  
 454 codes," in *Proc. DCC*, 2002, pp. 252–261.  
 455 [3] D. Slepian and J. K. Wolf, "Noiseless coding of correlated informa-  
 456 tion sources," *IEEE Trans. Inf. Theory*, vol. IT-19, no. 4, pp. 471–480,  
 457 Jul. 1973.  
 458 [4] B. Girod, A. Aaron, S. Rane, and D. Rebollo-Monedero, "Distributed  
 459 video coding," *Proc. IEEE*, vol. 93, no. 1, pp. 71–83, Jan. 2005.  
 460 [5] S. Draper, A. Khisti, E. Martinian, A. Vetro, and J. Yedidia, "Using  
 461 distributed source coding to secure fingerprint biometrics," in *Proc. IEEE*  
 462 *ICASSP*, Apr. 2007, vol. 2, pp. II-129–II-132.  
 463 [6] S. Pradhan and K. Ramchandran, "Distributed source coding using syn-  
 464 dromes (DISCUS): Design and construction," *IEEE Trans. Inf. Theory*,  
 465 vol. 49, no. 3, pp. 626–643, Mar. 2003.  
 466 [7] J. Garcia-Frias and Z. Xiong, "Distributed source and joint source-channel  
 467 coding: from theory to practice," in *Proc. IEEE ICASSP*, Mar. 2005,  
 468 vol. 5, pp. 1093–1096.  
 469 [8] J. Bajcsy and P. Mitran, "Coding for the Slepian–Wolf problem with  
 470 turbo codes," in *Proc. IEEE Global Telecommun. Conf.*, 2001, vol. 2,  
 471 pp. 1400–1404.

[9] J. Garcia-Frias, "Compression of correlated binary sources using turbo  
 472 codes," *IEEE Commun. Lett.*, vol. 5, no. 10, pp. 417–419, Oct. 2001. 473  
 [10] D. Varodayan, A. Aaron, and B. Girod, "Rate-adaptive codes for dis-  
 474 tributed source coding," *Elsevier Signal Process.*, vol. 86, no. 11, 475  
 pp. 3123–3130, Nov. 2006. 476  
 [11] A. Liveris, Z. Xiong, and C. Georghiades, "Compression of binary sources  
 477 with side information at the decoder using LDPC codes," *IEEE Commun.*  
 478 *Lett.*, vol. 6, no. 10, pp. 440–442, Oct. 2002. 479  
 [12] M. Sartipi and F. Fekri, "Distributed source coding using short to mod-  
 480 erate length rate-compatible LDPC codes: The entire slepian-wolf rate  
 481 region," *IEEE Trans. Commun.*, vol. 56, no. 3, pp. 400–411, Mar. 2008. 482  
 [13] J. Garcia-Frias and Y. Zhao, "Near-Shannon/Slepian–Wolf performance  
 483 for unknown correlated sources over AWGN channels," *IEEE Trans.*  
 484 *Commun.*, vol. 53, no. 4, pp. 555–559, Apr. 2005. 485  
 [14] Y. Zhao, W. Zhong, and J. Garcia-Frias, "Transmission of correlated  
 486 senders over a Rayleigh fading multiple access channel," *Elsevier Signal*  
 487 *Process.*, vol. 86, no. 11, pp. 3150–3159, Apr. 2006. 488  
 [15] J. Del Ser, P. Crespo, and A. Munoz, "Joint source-channel decoding  
 489 of correlated sources over ISI channels," in *Proc. IEEE VTC Spring*,  
 490 Jun. 2005, vol. 1, pp. 625–629. 491  
 [16] K. Anwar and T. Matsumoto, "Iterative spatial demapping for two corre-  
 492 lated sources with power control over fading MAC," in *Proc. IEEE VTC*  
 493 *Spring*, May 2012, pp. 1–7. 494  
 [17] L. Hanzo, T. H. Liew, B. L. Yeap, and S. X. Ng, *Turbo Coding, Turbo*  
 495 *Equalisation and Space-Time Coding: EXIT-Chart Aided Near-Capacity*  
 496 *Designs for Wireless Channels*. Hoboken, NJ, USA: Wiley, 2010. 497  
 [18] D. Varodayan, Y.-C. Lin, and B. Girod, "Adaptive distributed source  
 498 coding," *IEEE Trans. Image Process.*, vol. 21, no. 5, pp. 2630–2640,  
 499 May 2012. 500  
 [19] A. Roumy, K. Lajnef, and C. Guillemot, "Rate-adaptive turbo-  
 501 syndrome scheme for slepian-wolf coding," in *Proc. ACSSC*, Nov. 2007,  
 502 pp. 545–549. 503  
 [20] X. Lv, R. Liu, and R. Wang, "A novel rate-adaptive distributed source  
 504 coding scheme using polar codes," *IEEE Commun. Lett.*, vol. 17, no. 1,  
 505 pp. 143–146, Jan. 2013. 506  
 [21] L. Cui, S. Wang, S. Cheng, and M. Yeary, "Adaptive binary slepian-wolf  
 507 decoding using particle based belief propagation," *IEEE Trans. Commun.*,  
 508 vol. 59, no. 9, pp. 2337–2342, Sep. 2011. 509  
 [22] P. Robertson and T. Wörz, "Bandwidth-efficient turbo trellis-coded mod-  
 510 ulation using punctured component codes," *IEEE J. Sel. Areas Commun.*,  
 511 vol. 16, no. 2, pp. 206–218, Feb. 1998. 512  
 [23] V. Toto-Zaraso, A. Roumy, and C. Guillemot, "Rate-adaptive codes for  
 513 the entire slepian-wolf region and arbitrarily correlated sources," in *Proc.*  
 514 *IEEE ICASSP*, Apr. 2008, pp. 2965–2968. 515  
 [24] S. X. Ng and L. Hanzo, "On the MIMO channel capacity of multi-  
 516 dimensional signal sets," *IEEE Trans. Veh. Technol.*, vol. 55, no. 2,  
 517 pp. 528–536, Mar. 2006. 518



**Abdulah Jeza Aljohani** received the B.S. degree 519  
 (with honors) in electronics and communication en- 520  
 gineering from King Abdulaziz University, Jeddah, 521  
 Saudi Arabia, in 2006 and the M.Sc. degree (with 522  
 distinction) in wireless communications from the 523  
 University of Southampton, Southampton, U.K., in 524  
 2009. He is currently working toward the Ph.D. 525  
 degree with the Communications, Signal Processing, 526  
 and Control Group, School of Electronics and Com- 527  
 puter Science, University of Southampton. 528

His current research interests include joint source/ 529  
 channel coding and distributed source coding. 530



**Soon Xin Ng** (S'99–M'03–SM'08) received the B.Eng. degree (with first-class honors) in electronics engineering and the Ph.D. degree in wireless communications from the University of Southampton, Southampton, U.K., in 1999 and 2002, respectively.

From 2003 to 2006, he was a Postdoctoral Research Fellow working on collaborative European research projects known as SCOUT, NEWCOM, and PHOENIX. Since August 2006, he has been with the School of Electronics and Computer Science, University of Southampton, where he is currently a

Senior Lecturer. He is involved in the OPTIMIX and CONCERTO European projects, as well as the IU-ATC and UC4G projects. He is the author of over 150 papers and the coauthor of two John Wiley/IEEE Press books. His research interests include adaptive coded modulation, coded modulation, channel coding, space–time coding, joint source and channel coding, iterative detection, orthogonal frequency-division multiplexing, multiple-input–multiple-output systems, cooperative communications, distributed coding, quantum error-correcting codes, and joint wireless-and-optical-fiber communications.

Dr. Ng is a Chartered Engineer and a Fellow of the Higher Education Academy in the U.K.



**Lajos Hanzo** (F'08) received the M.S. degree in electronics, the D.Sc. degree, and the Doctor Honoris Causa degree from the Technical University of Budapest, Budapest, Hungary, in 1976, 1983, and 2009, respectively.

During his 37-year career in telecommunications, he has held various research and academic posts in Hungary, Germany, and the U.K. From 2008 to 2012, he was a Chaired Professor with Tsinghua University, Beijing, China. Since 1986, he has been with the School of Electronics and Computer Science,

University of Southampton, Southampton, U.K., where he is currently the Chair of telecommunications. He is the coauthor of 20 John Wiley/IEEE Press books on mobile radio communications, totalling in excess of 10 000 pages, and the author of more than 1300 research entries at IEEE Xplore. He has successfully supervised more than 80 Ph.D. students. He is an enthusiastic supporter of industrial and academic liaison, and he offers a range of industrial courses. Currently, he is directing a 100-strong academic research team, working on a range of research projects in the field of wireless multimedia communications sponsored by industry, the Engineering and Physical Sciences Research Council U.K., the European Research Council's Advanced Fellow Grant, and the Royal Society's Wolfson Research Merit Award. His research is funded by the European Research Council's Senior Research Fellow Grant. For further information on research in progress and associated publications, see (<http://www-mobile.ecs.soton.ac.uk>). He has 17 000 + citations.

Dr. Hanzo is a Fellow of the Royal Academy of Engineering, the Institution of Engineering and Technology, and the European Association for Signal Processing. He has served both as a Technical Program Committee and General Chair of IEEE conferences, has presented keynote lectures, and has been awarded a number of distinctions. He is also a Governor of the IEEE Vehicular Technology Society.

IEEE  
Proof

AUTHOR QUERY

NO QUERY.

IEEE  
Proof